Noname manuscript No.
(will be inserted by the editor)

Optimal strain-gauge placement for mechanical load estimation in circular cross-section shafts

X. Iriarte, J. Aginaga, G. Gainza, J. Ros, J. Bacaicoa

December 16, 2020

Abstract The customary electrical circuit configuration for estimating mechanical loads with strain gauges uses Wheatstone full- or half-bridges. For each mechanical load to be estimated, a dedicated bridge with two or four gauges has to be mounted, placing the strain gauges in specific configurations along the measured part. In this paper the strain of individual gauges is measured by means of quarter-bridges and all the mechanical loads exerted on a shaft are estimated jointly as different linear combinations of the strains of the gauges. The location of the gauges on the shaft are determined optimally and the influence of *apparent strain* related to temperature variations is avoided. Results show several configurations of reduced sets of gauges capable of optimally estimating the six components of the mechanical loads exerted on a circular cross-section shaft. The validation of the approach in a dedicated rig has shown the complexity of its experimental implementation.

Keywords Optimal Sensor Placement · Strain Gauges · Mechanical Loads · Estimation · Condition Monitoring

1 Introduction

Condition monitoring tries to identify changes in certain parameters of machinery and structures in order to prevent faults [23, 24]. Different types of sensors are placed in suitable locations of the machinery which measure, among others, the value of the parameters to be controlled, the external loads applied or the strain suffered by the materials. The type of sensors to be used, their location and the information reachable by their combination have been research topics in the last decades in several fields.

Due to their accuracy and low unit cost, strain gauges are one the most used sensors. They are bonded on the part of interest at locations where the strain is

Corresponding author: X. Iriarte
Institute of Smart Cities (ISC), Public University of Navarre, Iruñea-Pamplona, 31006, Spain.
Tel.: +34-948169286
E-mail: xabier.iriarte@unavarra.es

expected to be the largest. The gauges are commonly assembled in Wheatstone bridges which produce a voltage measurement related to the strain of the gauges [4, 14, 20].

Strain measurements are used to indirectly determine other properties as loads or deflections, which may not be directly measurable with a sensor. For example, Zhang *et al.* [22] use strain gauges to estimate bearing loads in rotating machinery with a so-called three section method, considering bending deflection with gauges located at the top and the bottom of a planar model of the shaft. Strain gauges have also been used in the design of force-sensors in one or more axis. A recent reference [19] presents a state-of-art review of multi-axis force sensors based on different strain sensing technologies, being strain gauges one of them. These force sensors typically use the strain due to bending loads to measure the loads. An example can be the dynamometer presented in [15], which uses bending strain in order to determine the cutting force in a machining process.

There are commonly accepted configurations of gauges used to measure bending, torsion or axial loads [6]. Fig. 1 illustrates the way gauges are usually placed, together with their corresponding Wheatstone bridge.

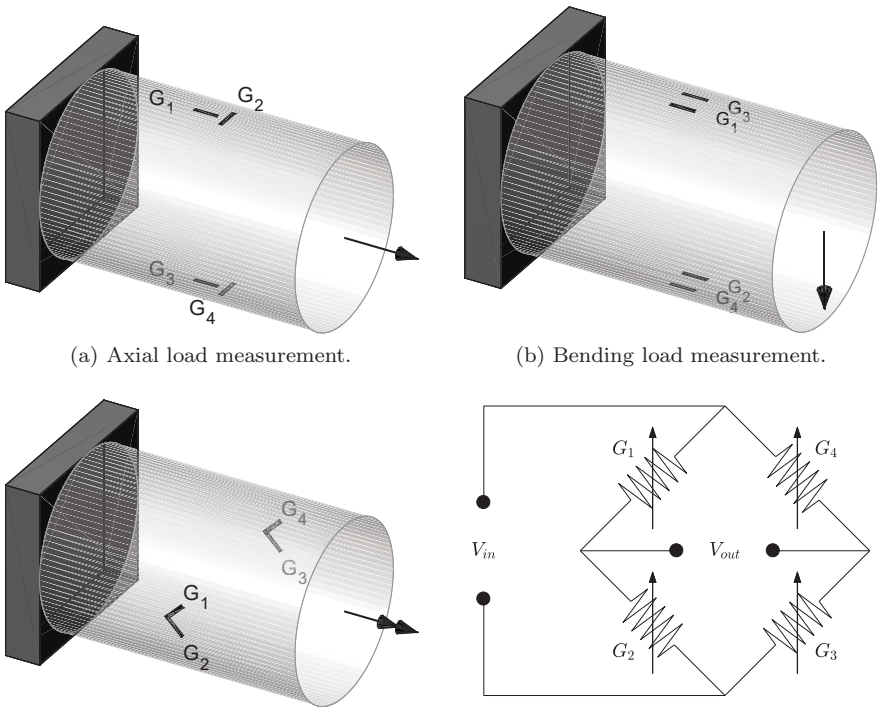

(a) Axial load measurement.

(b) Bending load measurement.

(c) Torsion load measurement.

(d) Wheatstone bridge configuration.

Fig. 1: Typical gauge configurations to measure specific loads.

Gauge configurations shown in Fig. 1 are useful since they measure specific load components while *compensating* for the other load components and thermal

strains. In other words, this means that the output of the Wheatstone bridge provides a voltage proportional to a single load component, regardless of the value of the other loads and thermal strains. For instance, the configuration in Fig. 1a can measure axial loads compensating for bending loads and torsion. In turn, the configuration in Fig. 1b measures bending loads compensating for axial and torsion loads. Finally, the configuration of Fig. 1c is used to measure torsion loads compensating for axial and bending loads. The three configurations of Fig. 1, when connected in a full-bridge as shown in Fig. 1d, compensate the thermal strain. This is a very important property associated with the configuration of the gauges and the way they are connected in the full bridge.

Despite the use of the configurations of gauges of Fig. 1 is very extended, they have the disadvantage of needing 4 strain gauges for measuring a single load. One could think that for measuring a single load a single gauge could be enough, but usually more than one gauge are needed in order to compensate for other loads and thermal strains. For example, a single gauge is required to measure bending loads, as in Fig. 2a, if the strain of the gauge is only produced by a pure bending moment. If there is also an axial load, the strain of the gauge is a combination of both bending and axial loads. Hence, in the presence of axial loads, at least 2 gauges are needed in order to measure the bending load compensating for the axial one. However, it is more common to use the configuration of Fig. 1b with 4 gauges because it improves the estimation sensitivity still compensating thermal effects.

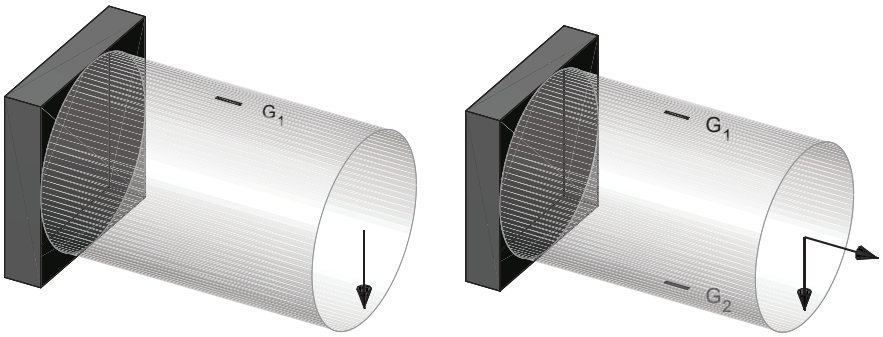

(a) A single gauge: when strain is due to a single bending load.

(b) Two gauges: when there is also an axial load.

Fig. 2: Configurations of gauges to measure bending loads.

Summarising, it is expected that a strain gauge which is arbitrarily located in a beam will be affected by each of the six components of a wrench (the three forces and three moments). With the customary configurations, a set of gauges is used in order to estimate a single component of the wrench, suppressing the contribution of the other components and compensating for thermal strains.

To the best of our knowledge, no one has considered measuring the whole wrench at the same time using a single set of gauges, in such a way that every gauge contributes to the measurement of every load. This paper shows a procedure

to optimise the location of the minimum set of gauges necessary to estimate the six components of the wrench, optionally compensating for thermal strains too. The estimation of each load is carried out using the contribution of every gauge and the optimal location of the gauges is calculated using the D-optimality criterion.

The paper is organised as follows. First, in Section 2 the strain of an arbitrarily located gauge is calculated, considering it is placed on the perimeter of the cross-section of a shaft. An explicit expression of the strain of the gauge is obtained as a function of the force and moment components of the external wrench at the specific section of the shaft. Section 3 shows how the wrench can be estimated from the strain measurement of a set of gauges. The location and orientation of the gauges around the section of the shaft are optimised in order to estimate wrench components with the minimum possible variance. Since the measurement of the gauge is affected also by temperature changes, Section 4 shows how temperature effects can be compensated. The results of the numerical optimisation, concerning the location of a set of gauges for estimating the external wrench at a section are presented in Section 5. Optimal results for measuring the wrench at a section with 6 and 8 gauges are also shown. Finally, the conclusions are presented in Section 8.

2 Determination of the strain of an arbitrarily located gauge

This section describes the determination of the strain of a single gauge as a function of the components of an external wrench. Using a set of bases, parameters and coordinates, the stress tensor at the location of the strain gauge is calculated first and then an explicit expression of the strain of the gauge is obtained as a function of components of the external wrench.

2.1 Measuring approach: full-bridges vs. quarter-bridges

As mentioned in the introduction, a key aspect of this work is that, instead of dedicating a set of gauges for each measured load component, a bigger set of gauges is dedicated to measure all wrench components. In the typical configurations, the strain gauges are assembled in a full- or half-bridge circuit configuration where a single voltage is measured.

The use of full Wheatstone bridges has some advantages over using half- or quarter-bridges. For example, as all the strain gauges are bonded to the same part, they are exposed to the same temperature. Since the Wheatstone bridge circuit electrically sums the resistance of two of the gauges and subtracts the resistance of the other two, any temperature effect is automatically compensated and temperature variations have no influence on the measurement of the loads.

Another advantage of using full Wheatstone bridges is related to the sensitivity. For example, the sensitivity of the full-bridge configuration of Fig. 1b for measuring bending moment is twice as sensitive as the half-bridge configuration of Fig. 2b since there are twice the gauges in the former. Therefore, two half-bridge would be equivalent to a full-bridge in terms of sensitivity.

Using quarter-bridges it is possible to reach the same result. If each of the 4 strain gauges of a full Wheatstone bridge was connected in a different quarter-bridge circuit, adding and subtracting the contribution of each of them mathemat-

ically (and not electrically as in the Wheatstone circuit) the same load results and sensitivities of the full-bridge would be achieved. This approach has an interesting advantage: the voltage drop measurement of a gauge in a quarter-bridge can be used to estimate several load components. That leads to a powerful outcome which is key in this paper: for a set of gauges, each of them in a quarter bridge, several load components can be calculated as different linear combinations of the voltage drops in the output of the quarter bridges.

In order to illustrate this, two ways of measuring torsion and shear will be explained:

1. Figs. 3a and 3b show the typical configurations in which the strain gauges are bonded in a shaft in order to measure torsion and shear, respectively. Figs. 3c and 3d represent their corresponding Wheatstone full-bridges. For these configurations torsion (M_1) and shear (F_3) are proportional to the corresponding output voltages, V_{out}^{Tor} and V_{out}^{Shear}, respectively. Likewise, these output voltages are proportional to linear combinations of the strains suffered by the gauges:

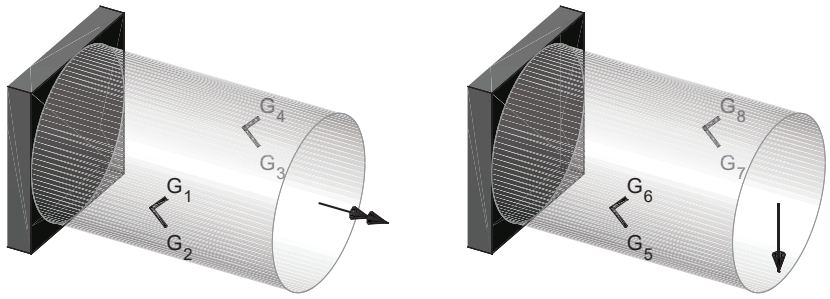

(a) Gauge configuration for Torsion.

(b) Gauge configuration for Shear.

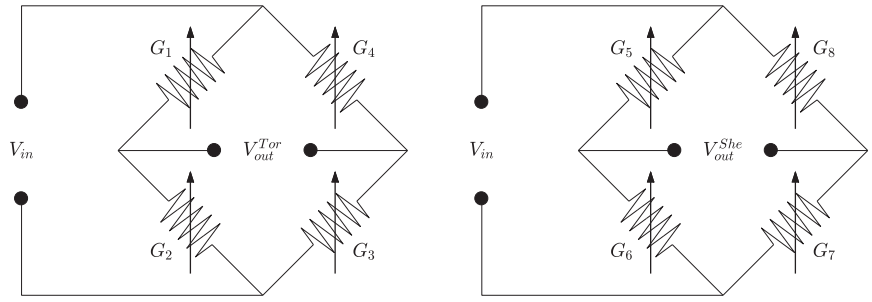

(c) Wheatstone bridge for Torsion.

(d) Wheatstone bridge for Shear.

Fig. 3: Typical configurations and Wheatstone bridges for measuring torsion and shear.

$$\begin{aligned} M_1 &\propto V_{out}^{Tor} \propto (\varepsilon_1 - \varepsilon_2 + \varepsilon_3 - \varepsilon_4) \\ F_3 &\propto V_{out}^{Shear} \propto (\varepsilon_5 - \varepsilon_6 + \varepsilon_7 - \varepsilon_8) \end{aligned} \tag{1}$$

where ε_i is the strain of the i^{th} gauge. If both shear and torsion estimations were desired, 2 full-bridges should be mounted using 8 strain gauges and 2 measuring channels.

2. On the other hand, with the 4 gauges of Fig. 3a, it is possible to measure both torsion and shear if the gauges are used in quarter-bridges, that is, a Wheatstone bridge for each strain gauge with three constant resistances as shown in Fig. 4. Considering that the output voltage is proportional to the deformation of the single gauge of the quarter-bridge, with each of the gauges of Fig. 3a plugged in an individual quarter-bridge, torsion (M_1) and shear (F_3) would be proportional to the linear combinations of the measured strains shown in Eq. (2):

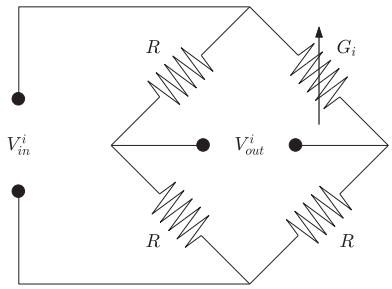

Fig. 4: Electric circuit of a Wheatstone quarter-bridge.

$$\begin{aligned} M_1 &\propto (V_{out}^1 - V_{out}^2 + V_{out}^3 - V_{out}^4) \propto (\varepsilon_1 - \varepsilon_2 + \varepsilon_3 - \varepsilon_4) \\ F_3 &\propto (V_{out}^1 - V_{out}^2 - V_{out}^3 + V_{out}^4) \propto (\varepsilon_1 - \varepsilon_2 - \varepsilon_3 + \varepsilon_4) \end{aligned} \tag{2}$$

With this approach, only 4 gauges are needed to measure torsion and shear, each of them with its corresponding quarter-bridge circuit.

This paper will follow the second approach. That is, the voltage drop that occurs in each individual strain gauge will be measured by means of a quarter-bridge circuit. Consequently, each component of the wrench will be calculated as a different linear combination of the quarter-bridge measurements.

2.2 Geometric modelling of the gauge location

The objective of this section is to build a geometric model to define the location and orientation of the strain gauges in the perimeter of a circular shaft as well as defining the bases used to determine the components of the wrench. For the sake of simplicity, the wrench will be calculated at the centre of the cross-section. The strain gauges will be located in a plane perpendicular to the axis of the shaft

and containing point O (*i.e.* in the perimeter of the perpendicular cross-section containing point O). As an optimal location of the strain gauges is desired, their location is unknown *a priori* and it will be described with two angular parameters that will determine the position and orientation of the gauge in the perimeter, as shown in Fig. 5.

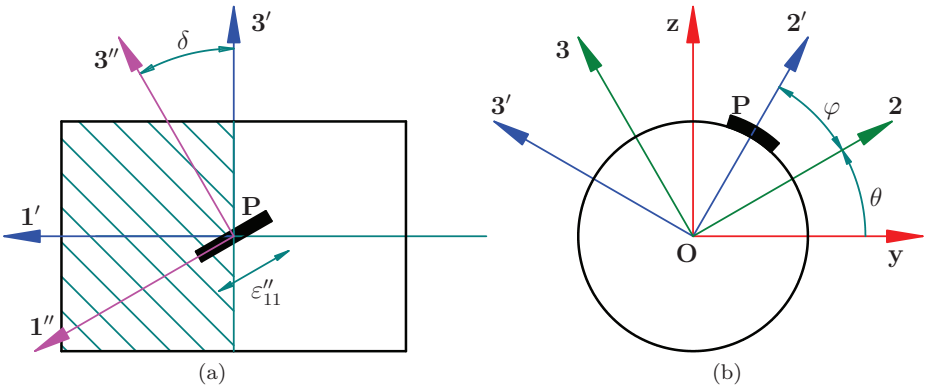

Fig. 5: Location and orientation of a strain gauge. Figure (a) is seen from $\mathbf{2}'$.

The cross section of the shaft is supposed to be constant in the vicinity of the considered section and is loaded with 3 forces and 3 moments that constitute the wrench with respect to point O. The material of the shaft is supposed to be linear, elastic and isotropic and *Saint Venant's Principle* is supposed to be met with the strain gauges located sufficiently far from the applied loads.

Four orientation bases, two angular parameters and a coordinate are used to determine the position and orientation of each strain gauge as described in Fig. 5. Base xyz is an orientation fixed to the ground and its positive x axis is coincident with the symmetry axis of the shaft. Angle θ determines the rotation of the shaft with respect to the ground and angle φ determines the position of the strain gauge at point P and the orientation of base $1'2'3'$. Angle δ determines the orientation of the strain gauge on the surface of the shaft. As the strain gauge is fixed to the shaft, bases 123, $1'2'3'$ and $1''2''3''$ are also fixed to the shaft. Bases $1'2'3'$ and $1''2''3''$ are different for each strain gauge since they depend on their own φ and δ angles. Conversely, bases xyz and 123 are common to all strain gauges.

As any vector or tensor is likely to be expressed in any of the bases defined, the proper coordinate transformation matrices will be defined. If the coordinates of vector $\mathbf{v}$ in base 123 are known to be $\{\mathbf{v}\}_{123}$ and its coordinates in base xyz are desired, $\{\mathbf{v}\}_{xyz}$, the coordinate transformation matrix $[\mathbf{R}]^{123}_{xyz}$ can be used as follows:

$$\{\mathbf{v}\}_{xyz} = \begin{bmatrix} 1 & 0 & 0 \\ 0 & \cos\theta & -\sin\theta \\ 0 & \sin\theta & \cos\theta \end{bmatrix}^{123}_{xyz} \{\mathbf{v}\}_{123} = [\mathbf{R}]^{123}_{xyz} \{\mathbf{v}\}_{123} \tag{3}$$

Analogously, the next two coordinate transformation matrices can be defined:

$$\{\mathbf{v}\}_{123} = \begin{bmatrix} 1 & 0 & 0 \\ 0 & \cos\varphi & -\sin\varphi \\ 0 & \sin\varphi & \cos\varphi \end{bmatrix}_{123}^{1'2'3'} \{\mathbf{v}\}_{1'2'3'} = [\mathbf{R}]_{123}^{1'2'3'} \{\mathbf{v}\}_{1'2'3'} \tag{4}$$

$$\{\mathbf{v}\}_{1'2'3'} = \begin{bmatrix} \cos\delta & 0 & \sin\delta \\ 0 & 1 & 0 \\ -\sin\delta & 0 & \cos\delta \end{bmatrix}_{1'2'3'}^{1''2''3''} \{\mathbf{v}\}_{1''2''3''} = [\mathbf{R}]_{1'2'3'}^{1''2''3''} \{\mathbf{v}\}_{1''2''3''} \tag{5}$$

In what follows these transformation matrices will be used because the strain of each gauge is measured in its own $1''2''3''$ base while the components of the wrench are desired in bases 123 or xyz.

2.3 Stress tensor components calculation for an arbitrary wrench

The wrench that is to be estimated is the one that the right half of the shaft in Fig. 5a exerts on the left half. The components of the force and moment of this wrench in bases 123 and $1'2'3'$ are related to each other as:

$$\begin{Bmatrix} F_1' \\ F_2' \\ F_3' \end{Bmatrix}_{1'2'3'} = \begin{bmatrix} 1 & 0 & 0 \\ 0 & \cos\varphi & \sin\varphi \\ 0 & -\sin\varphi & \cos\varphi \end{bmatrix}_{1'2'3'}^{123} \begin{Bmatrix} F_1 \\ F_2 \\ F_3 \end{Bmatrix}_{123} = \begin{Bmatrix} F_1 \\ F_2\cos\varphi + F_3\sin\varphi \\ -F_2\sin\varphi + F_3\cos\varphi \end{Bmatrix}_{1'2'3'} \tag{6}$$

$$\begin{Bmatrix} M_1' \\ M_2' \\ M_3' \end{Bmatrix}_{1'2'3'} = \begin{bmatrix} 1 & 0 & 0 \\ 0 & \cos\varphi & \sin\varphi \\ 0 & -\sin\varphi & \cos\varphi \end{bmatrix}_{1'2'3'}^{123} \begin{Bmatrix} M_1 \\ M_2 \\ M_3 \end{Bmatrix}_{123} = \begin{Bmatrix} M_1 \\ M_2\cos\varphi + M_3\sin\varphi \\ -M_2\sin\varphi + M_3\cos\varphi \end{Bmatrix}_{1'2'3'} \tag{7}$$

where F_1 denotes axial force, F_2 and F_3 denote shear forces, M_1 denotes torsion moment and M_2 and M_3 denote bending moments with respect to point O. Even if wrench components will be given in base 123, for the stress tensor calculation the components in base $1'2'3'$ will be used first.

Let $\mathbf{t}' = (F_1', F_2', F_3', M_1', M_2', M_3')^T$ be the external wrench at point O. In order to calculate the stress tensor $\overline{\overline{\boldsymbol{\sigma}}}$ at point P related to the external wrench $\mathbf{t}'$, the stress tensors related to the individual components of the wrench are determined first. The compound stress tensor will be calculated by superposition of the individual ones. For the solid differential shown in Fig. 6a, the defined wrench is the one that is applied to the hatched face.

The stress tensor components are established by defining the three mutually orthogonal surfaces at point P. The normals to each surface will establish, in this case, the $1'$, $2'$ and $3'$ Cartesian axes. In general, each surface will have a normal and two shear stresses. The normal stress is labelled σ and the shear stresses acting on the surface are labelled τ. In the double subscript notation, the first subscript indicates the direction normal to the surface whereas the second subscript is the direction of the stress. By convention, the normal stress is positive if its direction is outwards the differential cube (traction). In a similar manner, the shear stresses in the *positive sides*[1] of the differential cube will be positive when they point in the positive direction of base axis. As the stress tensor is symmetric, $\tau_{ij} = \tau_{ji}$, $\forall\, i \neq j$.

[1] *Positive sides* of the cube are those where the outwards perpendicular vector coincides in direction with the positive direction of an axis of the base.

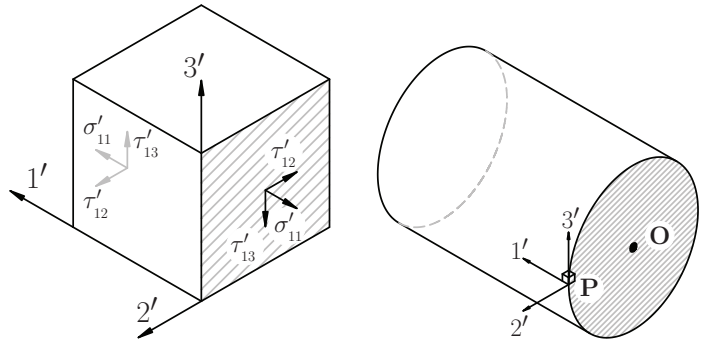

(a) Solid differential and stress tensor components.

(b) Solid differential in the shaft.

Fig. 6: Stress tensor components in the differential at point P.

- Effect of the axial force: an axial force F_1' exerted in the positive direction of axis $1'$ causes a compression stress in the whole section. Therefore, the stress tensor at point P related to the axial force will be:

$$[\overline{\overline{\boldsymbol{\sigma}}}_{F_1'}]_{1'2'3'} = \begin{bmatrix} -\frac{F_1'}{A} & 0 & 0 \\ & 0 & 0 \\ & & 0 \end{bmatrix}_{1'2'3'} \tag{8}$$

  where A is the area of the section.
- Effect of the bending moment: a bending moment M_3' exerted in the positive direction of axis $3'$ causes a traction stress at point P. Therefore, the stress tensor related to this bending moment will be:

$$[\overline{\overline{\boldsymbol{\sigma}}}_{M_3'}]_{1'2'3'} = \begin{bmatrix} \frac{M_3'}{w} & 0 & 0 \\ & 0 & 0 \\ & & 0 \end{bmatrix}_{1'2'3'} \tag{9}$$

  where w is the sectional modulus.
- Effect of the shear force: according to *Timoshenko's Beam Theory* [7], a shear force F_3' exerted in the positive direction of axis $3'$ causes a negative shear stress at point P equal to:

$$\tau_{13}' = -\frac{F_3'}{kA} \tag{10}$$

  where k is the *shear coefficient* that represents the ratio of the average shear stress on a section to the shear stress at the centroid. For hollow circle cross sections k takes the following expression [3]:

$$k = \frac{6\,(1+\nu)(1+m^2)^2}{(7+6\nu)(1+m^2)^2 + (20+12\nu)m^2} \tag{11}$$

  where ν is *Poisson's modulus*, $m = \frac{r}{R}$, and r and R are the inner and outer radii, respectively. This expression is also valid for full circle cross sections making $r = 0$ and thin-walled round tube sections making $r = R$.

Therefore, the stress tensor related to the shear force can be written as:

$$[\overline{\overline{\boldsymbol{\sigma}}}_{F_3'}]_{1'2'3'} = \begin{bmatrix} 0 & 0 & -\frac{F_3'}{kA} \\ & 0 & 0 \\ & & 0 \end{bmatrix}_{1'2'3'} \tag{12}$$

- Effect of the torsion moment: a torsion moment M_1' exerted in the positive direction of axis $1'$ causes a negative shear stress at point P. Therefore, the stress tensor related to the torsion moment will be:

$$[\overline{\overline{\boldsymbol{\sigma}}}_{M_1'}]_{1'2'3'} = \begin{bmatrix} 0 & 0 & -\frac{M_1'R}{I_p} \\ & 0 & 0 \\ & & 0 \end{bmatrix}_{1'2'3'} \tag{13}$$

  where I_p is the *polar moment of inertia* of the section.
- Components F_2' and M_2' do not cause any stress at point P.

The superposition of the 6 stress tensors gives the compound stress tensor for the wrench, $[\overline{\overline{\boldsymbol{\sigma}}}]_{1'2'3'}$, expressed in base $1'2'3'$. The stress tensor is symmetric.

$$[\overline{\overline{\boldsymbol{\sigma}}}(\mathbf{t}')]_{1'2'3'} = \begin{bmatrix} -\frac{F_1'}{A} + \frac{M_3'}{w} & 0 & -\frac{M_1'R}{I_P} - \frac{F_3'}{kA} \\ & 0 & 0 \\ & & 0 \end{bmatrix}_{1'2'3'} = \begin{bmatrix} \sigma_{11}' & \tau_{12}' & \tau_{13}' \\ & \sigma_{22}' & \tau_{23}' \\ & & \sigma_{33}' \end{bmatrix}_{1'2'3'} \tag{14}$$

2.4 Strain calculation for an arbitrarily located gauge and an arbitrary wrench

In order to calculate the strain tensor $\overline{\overline{\boldsymbol{\varepsilon}}}$ in terms of the stress tensor $\overline{\overline{\boldsymbol{\sigma}}}$, their components can be written in column vector form:

$$\begin{aligned} \overline{\boldsymbol{\sigma}} &= \left(\sigma_{11}', \sigma_{22}', \sigma_{33}', \tau_{12}', \tau_{23}', \tau_{13}'\right)^T \\ \overline{\boldsymbol{\varepsilon}} &= \left(\varepsilon_{11}', \varepsilon_{22}', \varepsilon_{33}', \varepsilon_{12}', \varepsilon_{23}', \varepsilon_{13}'\right)^T \end{aligned} \tag{15}$$

where the components of the symmetric strain tensor are:

$$[\overline{\overline{\boldsymbol{\varepsilon}}}]_{1'2'3'} = \begin{bmatrix} \varepsilon_{11}' & \varepsilon_{12}' & \varepsilon_{13}' \\ & \varepsilon_{22}' & \varepsilon_{23}' \\ & & \varepsilon_{33}' \end{bmatrix}_{1'2'3'} \tag{16}$$

In vector form, the following relation between strain and stress holds:

$$\overline{\boldsymbol{\sigma}} = \mathbf{D}\overline{\boldsymbol{\varepsilon}} \tag{17}$$

Assuming that the material is linear, elastic and isotropic, $\mathbf{D}$ can be written as

$$\mathbf{D} = \frac{E}{(1+\nu)(1-2\nu)} \begin{bmatrix} 1-\nu & \nu & \nu & 0 & 0 & 0 \\ & 1-\nu & \nu & 0 & 0 & 0 \\ & & 1-\nu & 0 & 0 & 0 \\ & & & 1-2\nu & 0 & 0 \\ & & & & 1-2\nu & 0 \\ & & & & & 1-2\nu \end{bmatrix} \tag{18}$$

where constants E and ν are the *Young's* and *Poisson's moduli*, respectively.

Since the strain gauge is aligned with axis $1''$, the strain tensor will be expressed in base $1''2''3''$ as follows:

$$[\overline{\overline{\varepsilon}}]_{1''2''3''} = [\mathbf{R}]^{1'2'3'}_{1''2''3''} [\overline{\overline{\varepsilon}}]_{1'2'3'} [\mathbf{R}]^{1''2''3''}_{1'2'3'} \tag{19}$$

Taking the $(1,1)$ component, the strain of the gauge, ε, can be obtained.

$$\varepsilon = \varepsilon''_{11} \tag{20}$$

Up to now, the stress tensor and the strain of the gauge have been written in terms of $\mathbf{t}'$. Let us define vector $\mathbf{t} = (F_1, F_2, F_3, M_1, M_2, M_3)^T$. Using the Eqs. (6) and (7) that relate the components of the wrench in bases 123 and $1'2'3'$, the strain of the gauge is written in terms of $\mathbf{t}$. As ε is linear in $\mathbf{t}$, it can be written as:

$$\varepsilon = \frac{\partial \varepsilon}{\partial \mathbf{t}} \mathbf{t} = \mathbf{w}\mathbf{t} \tag{21}$$

where the explicit expression of the row vector $\mathbf{w}$ is:

$$\mathbf{w}(\varphi, \delta) = \left\{ \begin{array}{c} \frac{(1+\nu)\sin^2\delta - 1}{EA} \\ -\frac{2(\nu+1)\cos\delta \sin\delta \sin\varphi}{kEA} \\ \frac{2(\nu+1)\cos\delta \sin\delta \cos\varphi}{kEA} \\ \frac{R(\nu+1)\sin 2\delta}{EI_p} \\ \frac{((1+\nu)\sin^2\delta - 1)\sin\varphi}{Ew} \\ -\frac{((1+\nu)\sin^2\delta - 1)\cos\varphi}{Ew} \end{array} \right\}^T \tag{22}$$

Therefore, for a gauge located at an arbitrary point defined by φ and δ, Eq. (21) provides the strain of the gauge related to an arbitrary wrench $\mathbf{t}$.

3 Optimum estimation of the wrench

In the previous section, it has been shown how to calculate the strain of a gauge under the action of a wrench. In contrast, this section shows how the wrench can be estimated from the strain measurements of a set of gauges. Moreover, it will be shown how to determine the optimal configuration of the gauges to estimate the wrench. For the sake of simplicity, thermal strain will not be considered in this section and will be addressed in Section 4.

3.1 Estimation of the wrench in terms of the strain of several gauges

Let us suppose that wrench $\mathbf{t}$ has to be estimated from strain measurements. As the wrench has $p = 6$ components it will be necessary to use, at least, p strain gauges in order to estimate each of the individual components. Let $n \geq p$ be the number of strain gauges located along the perimeter of a certain cross-section of the shaft. Let us denote by ε_i the strain of the i^{th} gauge and let φ_i and δ_i be the angles that determine the position and orientation of the i^{th} strain gauge

$(i = 1, \ldots, n)$ as defined in Fig. 5. Then, the following system of equations can be written:

$$\begin{Bmatrix} \varepsilon_1 \\ \varepsilon_2 \\ \vdots \\ \varepsilon_n \end{Bmatrix} = \begin{bmatrix} \mathbf{w}_1 \\ \mathbf{w}_2 \\ \vdots \\ \mathbf{w}_n \end{bmatrix} \begin{Bmatrix} F_1 \\ F_2 \\ F_3 \\ M_1 \\ M_2 \\ M_3 \end{Bmatrix} \tag{23}$$

where $\mathbf{w}_i = \mathbf{w}(\varphi_i, \delta_i)$. Gathering the n mechanical strains in vector $\boldsymbol{\varepsilon}$ and the n row vectors $\mathbf{w}_i$ in $\mathbf{W}$, Eq. (23) can be rewritten as:

$$\boldsymbol{\varepsilon} = \mathbf{W}(\boldsymbol{\vartheta})\,\mathbf{t} \tag{24}$$

where $\boldsymbol{\varphi} = (\varphi_1, \varphi_2, \ldots, \varphi_n)$, $\boldsymbol{\delta} = (\delta_1, \delta_2, \ldots, \delta_n)$ and $\boldsymbol{\vartheta} = (\boldsymbol{\varphi}, \boldsymbol{\delta})$. Matrix $\mathbf{W} = \mathbf{W}(\boldsymbol{\vartheta})$ represents the $n \times p$ observation matrix which has all the information of the location of the gauges. Measuring the strain of the gauges for an instant and writing $\mathbf{W}$ for the configuration of the gauges, one could solve the linear system of Eq. (24) to calculate $\mathbf{t}$ in terms of $\boldsymbol{\varepsilon}$, assuming $\mathbf{W}$ has full rank.

However, in an experimental framework, vector $\boldsymbol{\varepsilon}$ will be measured with error and it will be appropriate to use Linear Regression Theory [5] to get *estimates* for $\mathbf{t}$ and the variance of $\mathbf{t}$. We will refer to them as $\hat{\mathbf{t}}$ and $var(\hat{\mathbf{t}})$, respectively.

Let us write a typical statistical linear model in which the measured strain vector, $\boldsymbol{\varepsilon}_m$, is written as the sum of the *true* mechanical strain, $\boldsymbol{\varepsilon}$, and the global measurement uncertainty, $\mathbf{e}$:

$$\boldsymbol{\varepsilon}_m = \mathbf{W}\mathbf{t} + \mathbf{e} \tag{25}$$

where both $\boldsymbol{\varepsilon}_m$ and $\mathbf{e}$ are random variables [10,12] and $\mathbf{W}$ is deterministic, *i.e.* known without uncertainty. For the sake of simplicity, it will be assumed now that the expectation of $\mathbf{e}$ is null, *i.e.*, $E[\mathbf{e}] = \mathbf{0}$. It is important to emphasise that this assumption can only be valid if a proper calibration of the gauges is performed [2]. The results below this point are not useful for a real implementation without the calibration of the strain gauges. However this issue will not be tackled in this paper owing to lack of space.

In this situation, the minimum variance *Weighted Least Squares Estimator* for $\mathbf{t}$ coincides with the *Maximum Likelihood Estimator* [1,5,12,18]:

$$\hat{\mathbf{t}} = \left(\mathbf{W}^T\boldsymbol{\Sigma}^{-1}\mathbf{W}\right)^{-1}\mathbf{W}^T\boldsymbol{\Sigma}^{-1}\boldsymbol{\varepsilon}_m \tag{26}$$

where $\boldsymbol{\Sigma} = E[\mathbf{e}\mathbf{e}^T]$ is the covariance matrix of $\mathbf{e}$. As $\boldsymbol{\varepsilon}_m$ is a random variable, the estimation of $\mathbf{t}$, $\hat{\mathbf{t}}$, will also be a random variable. The estimate in Eq. (26) is also known as the *Markov Estimate* or the *Best Linear Unbiased Estimate* [8,12].

From Eqs. (25) and (26) expression $(\hat{\mathbf{t}} - \mathbf{t})$ can be written as:

$$\hat{\mathbf{t}} - \mathbf{t} = \left(\mathbf{W}^T\boldsymbol{\Sigma}^{-1}\mathbf{W}\right)^{-1}\mathbf{W}^T\boldsymbol{\Sigma}^{-1}\mathbf{e} \tag{27}$$

and the estimator will be unbiased ($E[\hat{\mathbf{t}} - \mathbf{t}] = \mathbf{0}$) if $E[\mathbf{e}] = \mathbf{0}$.

Likewise, the variance of $\hat{\mathbf{t}}$ can be written as:

$$var(\hat{\mathbf{t}}) = E[(\hat{\mathbf{t}} - \mathbf{t})(\hat{\mathbf{t}} - \mathbf{t})^T] = \left(\mathbf{W}^T\boldsymbol{\Sigma}^{-1}\mathbf{W}\right)^{-1} \tag{28}$$

If all the strain gauges are of the same type, it can be assumed that the variance of their measurement uncertainty will be the same. Therefore,

$$\mathbf{\Sigma} = var(\mathbf{e}) = var(\boldsymbol{\varepsilon}_m) = var(\varepsilon_m)\,\mathbf{I}_n \tag{29}$$

where $var(\varepsilon_m)$ is the variance of the individual strain gauges and $\mathbf{I}_n$ is the $n \times n$ identity matrix. Then, the estimator of $\mathbf{t}$ given in Eq. (26) simplifies to:

$$\hat{\mathbf{t}} = \left(\mathbf{W}^T\mathbf{W}\right)^{-1}\mathbf{W}^T\boldsymbol{\varepsilon}_m \tag{30}$$

As the gauges are bonded, $\mathbf{W}(\boldsymbol{\vartheta})$ will be a constant matrix. Therefore, if expression $\left(\mathbf{W}^T\mathbf{W}\right)^{-1}\mathbf{W}^T$ is computed offline, the real-time estimation of the wrench will only require a matrix by vector multiplication, making the estimation of the wrench very efficient.

Assuming Eq. (29) holds, the variance of the estimated wrench simplifies to:

$$var(\hat{\mathbf{t}}) = var(\varepsilon_m)\left(\mathbf{W}^T\mathbf{W}\right)^{-1} \tag{31}$$

and will only have to be computed once.

For $n > p$, the variance of the measured strains can be estimated as [12]:

$$\widehat{var(\varepsilon_m)} = \frac{(\boldsymbol{\varepsilon}_m - \mathbf{W}\hat{\mathbf{t}})^T(\boldsymbol{\varepsilon}_m - \mathbf{W}\hat{\mathbf{t}})}{n-p} \tag{32}$$

Making use of N different measurements of the strain vector, a more precise estimation of the variance can be calculated:

$$\widehat{var(\varepsilon_m)} = \frac{\sum_{k=1}^{N}(\boldsymbol{\varepsilon}_m^k - \mathbf{W}\hat{\mathbf{t}}^k)^T(\boldsymbol{\varepsilon}_m^k - \mathbf{W}\hat{\mathbf{t}}^k)}{N(n-p)} \tag{33}$$

where $\boldsymbol{\varepsilon}_m^k$ and $\hat{\mathbf{t}}^k$ are the k^{th} strain measure and wrench estimation, respectively.

3.2 Optimum estimation of wrench components

The main purpose of the paper is to determine the location of the strain gauges for an optimal wrench estimation. Thus, an optimality criterion has to be settled in order to determine that a gauge configuration is better than another. In this context, D-optimality is the best observability index for maximising the observability of the wrench [17]. Moreover, this criterion is *scaling invariant*, so it is insensitive to the different dimensions of the components of the wrench (forces and moments).

D-Optimality has been used in several references such as [9,11,16] in the context of *Optimal Sensor Placement*. These references describe optimisation procedures based on the *Fisher information matrix* [8] for optimising different sensor locations. One of the first works in this context is [21], in which a methodology for parameter identification is presented optimising the location of the sensors for different numbers of sensors. In [13] a methodology for optimal sensor placement based on the *Fisher information matrix* is presented and the effect that the damage in the structure has in the sensors performance is also investigated.

Assuming Eq. (29) holds, and dropping the scaling factor $var(\varepsilon_m)$, the cost function $\mathcal{F}$ of the D-optimality criterion can be written as [12,18]:

$$\mathcal{F}(\mathbf{W}) = -\log(\det(\mathbf{W}^T\mathbf{W})) \tag{34}$$

Derivation of Eq. (34) is explained in detail in [18], where Swevers *et al.* solve the problem of trajectory optimisation for dynamic parameter estimation in robotics. The determination of the *trajectory parameters* in that paper is analogous to the determination of the *gauges location* in the present paper.

Finally, once the optimality criterion is established, in order to determine the optimal location and orientation of the strain gauges, $\boldsymbol{\vartheta}^{opt}$, it would suffice to solve the following minimisation problem:

$$\boldsymbol{\vartheta}^{opt} = \arg_{\boldsymbol{\vartheta}} \min(\mathcal{F}(\mathbf{W}(\boldsymbol{\vartheta}))), \quad \text{subject to } \mathbf{c}(\boldsymbol{\vartheta}) = \mathbf{0}, \tag{35}$$

where $\mathbf{c}(\boldsymbol{\vartheta}) = \mathbf{0}$ are optional non-linear constraints. For example, these constraints could be used to force two gauges to be bonded in the same φ angle and their δ angles to be shifted 90°. This would lead to use *X Rosettes* [6] instead of individual gauges.

Note that vector $\boldsymbol{\vartheta}^{opt}$ determines the optimum location and orientation of the strain gauges for the wrench estimation with the minimum possible variance.

4 Wrench estimation with temperature compensation

If a measurement is performed when the temperature differs from the one present during the calibration, a temperature induced strain will occur. This temperature response is reversible and the effects disappear when the gauges are at the calibration temperature. In the literature, this temperature response is often called *apparent strain* [6].

There are many factors affecting the temperature response [4,6,14]. Both the material of the measuring-grid of the strain gauges and the material of the part where the gauge is bonded, will have their own *thermal expansion coefficient*. Thus, when a temperature change occurs, both materials will expand/contract and will cause a strain not related to mechanical loads. Moreover, the *electrical resistance coefficients* of the materials of the gauges and wires also depend on temperature, leading to an additional contribution to the *apparent strain*.

In order to minimise these thermal effects, *temperature-compensated strain gauges* can be used [14]. This type of strain gauges are designed with a thermal coefficient that compensates (as far as possible) these thermal effects. These gauges are only useful if bonded on materials with a specific thermal expansion coefficient. However, complete compensation is not possible with these gauges for a continuous range of temperatures because the thermal expansion coefficients of the materials and the temperature coefficient of the electrical resistance of the material of the gauge both depend on temperature.

One efficient way of compensating the temperature effects relies on using various strain gauges. Choosing a suitable configuration, the mechanical loads can be calculated making the temperature response of the different gauges compensate each other.

In order to follow this approach, let us suppose that the gauges will sense certain strain related to the temperature variations, $\boldsymbol{\varepsilon}_T$. This strain will be indistinguishable from the strain related to mechanical loads, $\boldsymbol{\varepsilon}$. In order to take into account the temperature variations, the measured strains, $\boldsymbol{\varepsilon}_m$, should be written as:

$$\boldsymbol{\varepsilon}_m = \boldsymbol{\varepsilon} + \boldsymbol{\varepsilon}_T + \mathbf{e}. \tag{36}$$

Assuming that any possible temperature effect affects the measurement of all the strain gauges in the same way[2], the temperature strain could be written as $\boldsymbol{\varepsilon}_T = \mathbf{1}\varepsilon_T$, where $\mathbf{1}$ represents an $n \times 1$ vector of ones and ε_T is an unknown scalar. Substituting $\boldsymbol{\varepsilon} = \mathbf{W}\mathbf{t}$ and $\boldsymbol{\varepsilon}_T = \mathbf{1}\varepsilon_T$ in Eq. (36), one gets:

$$\boldsymbol{\varepsilon}_m = \begin{bmatrix}\mathbf{W} & \mathbf{1}\end{bmatrix} \begin{Bmatrix}\mathbf{t} \\ \varepsilon_T\end{Bmatrix} + \mathbf{e}. \tag{37}$$

We could refer to Eq. (37) as the *extended system of equations* where the temperature strain has been taken into account. This linear system is analogous to Eq. (25) where matrix $\mathbf{W}$ and vector $\mathbf{t}$ have been extended with a column and a row, respectively. Therefore, the estimation and optimisation procedures presented before can also be applied to the extended system.

5 Results and discussion

In Sections 3 and 4, a procedure to find the optimal location of a set a gauges on the perimeter of a circular cross-section shaft has been developed. The procedure can be applied in order to find the optimal location of a set of $n \geq p$ gauges for estimating all the components of $\mathbf{t}$, with ($p = 7$) or without ($p = 6$) temperature compensation. This section describes the results obtained from the application of the developed procedure.

5.1 Estimating $\mathbf{t}$ with 6 strain gauges

If no temperature compensation is desired, it is sufficient to use 6 strain gauges in order to estimate the 6 components of $\mathbf{t}$. The optimisation procedure of Section 3 has been applied for several different values of the geometric (A, w, I_p, R, k) and material (E, ν) parameters. An analysis of the results reveals that the structure of the solutions has the following form:

$$\begin{aligned}\boldsymbol{\varphi}^{opt} &= (0^\circ, 0^\circ, 120^\circ, 120^\circ, 240^\circ, 240^\circ) + (\varphi_a, \varphi_b, \varphi_a, \varphi_b, \varphi_a, \varphi_b) \\ \boldsymbol{\delta}^{opt} &= (\ \ \alpha, -\alpha, \quad \alpha, -\alpha, \quad \alpha, -\alpha)\end{aligned} \tag{38}$$

On the one hand, the optimal value of α is observed to be different for different values of the geometric and material parameters. On the other hand, this solution is optimal for any value of φ_a and φ_b and a particularly convenient configuration

[2] All the gauges are equal (same material properties and geometry) the temperature variations are the same for all gauges, the wires connecting the gauges are equal (same material properties and geometry) all the gauges are bonded to the same material, etc. These conditions are commonly met when measuring with strain gauges.

is obtained for $\varphi_a = \varphi_b = 0$. In this situation we can consider the optimal configuration as three couples of gauges that are bonded along the perimeter with the same φ while the angle between couples is 120°. Moreover, the orientations of the gauges of each couple are given by $+\alpha$ and $-\alpha$.

Evaluating matrix $\mathbf{W}$ in this configuration for a symbolic α and symbolic representations of the geometric and material parameters, the expression for the optimisation criterion of Eq. (34) can be obtained.

$$\begin{aligned}\mathcal{F}(\mathbf{W}) = &- \log\left(4\,(\nu+1)^6 \sin^6 2\alpha \left(\cos^2\alpha - \nu\sin^2\alpha\right)^6\right) \\ &- \log\left(\frac{3^6\,R^4}{k^4\,A^6\,E^{12}\,I_p^2\,w^4}\right)\end{aligned} \tag{39}$$

From this expression it is obvious that the optimum α depends only on ν as the second term in Eq. (39) has no influence on the α that minimises $\mathcal{F}$.

The dependence of α^{opt} (the optimum α) on ν has been analysed and the outcome is that, for typical values of Poisson's modulus for common metals, namely from 0.25 to 0.40, the value of α^{opt} varies from 28° to 26° which can be considered a small variation.

Fig. 7 represents the optimisation criterion in terms of α for $\nu = \frac{1}{3}$ where the optimum gauge orientation is $\alpha^{opt} = 26.8°$.

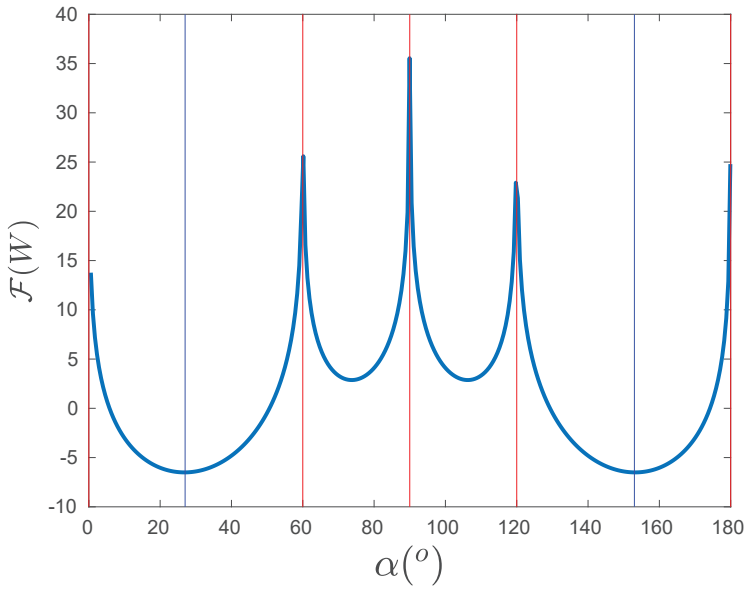

Fig. 7: Optimisation criterion value in terms of α for $\nu = \frac{1}{3}$.

Evaluating matrix $\mathbf{W}$ and $\mathbf{W}^{-1}$ with the values of $\boldsymbol{\varphi}^{opt}$ and $\boldsymbol{\delta}^{opt}$ of Eq. (38), for $\varphi_a = \varphi_b = 0$, the following expressions are obtained:

$$\mathbf{W} = \begin{bmatrix} \frac{-f(\alpha,\nu)}{AE} & 0 & \frac{g(\alpha,\nu)}{kAE} & \frac{R\,g(\alpha,\nu)}{E\,\mathrm{I_p}} & 0 & \frac{f(\alpha,\nu)}{E\,w} \\ \frac{-f(\alpha,\nu)}{AE} & 0 & -\frac{g(\alpha,\nu)}{kAE} & -\frac{R\,g(\alpha,\nu)}{E\,\mathrm{I_p}} & 0 & \frac{f(\alpha,\nu)}{E\,w} \\ \frac{-f(\alpha,\nu)}{AE} & -\frac{\sqrt{3}\,g(\alpha,\nu)}{2kAE} & -\frac{g(\alpha,\nu)}{2kAE} & \frac{R\,g(\alpha,\nu)}{E\,\mathrm{I_p}} & -\frac{\sqrt{3}\,f(\alpha,\nu)}{2Ew} & -\frac{f(\alpha,\nu)}{2Ew} \\ \frac{-f(\alpha,\nu)}{AE} & \frac{\sqrt{3}\,g(\alpha,\nu)}{2kAE} & \frac{g(\alpha,\nu)}{2kAE} & -\frac{R\,g(\alpha,\nu)}{E\,\mathrm{I_p}} & -\frac{\sqrt{3}\,f(\alpha,\nu)}{2Ew} & -\frac{f(\alpha,\nu)}{2Ew} \\ \frac{-f(\alpha,\nu)}{AE} & \frac{\sqrt{3}\,g(\alpha,\nu)}{2kAE} & -\frac{g(\alpha,\nu)}{2kAE} & \frac{R\,g(\alpha,\nu)}{E\,\mathrm{I_p}} & \frac{\sqrt{3}\,f(\alpha,\nu)}{2\,E\,w} & -\frac{f(\alpha,\nu)}{2Ew} \\ \frac{-f(\alpha,\nu)}{AE} & -\frac{\sqrt{3}\,g(\alpha,\nu)}{2kAE} & \frac{g(\alpha,\nu)}{2kAE} & -\frac{R\,g(\alpha,\nu)}{E\,\mathrm{I_p}} & \frac{\sqrt{3}\,f(\alpha,\nu)}{2Ew} & -\frac{f(\alpha,\nu)}{2Ew} \end{bmatrix} \tag{40}$$

$$\mathbf{W}^{-1} = \begin{bmatrix} \frac{-AE}{6\,f(\alpha,\nu)} & \frac{-AE}{6\,f(\alpha,\nu)} & \frac{-AE}{6\,f(\alpha,\nu)} & \frac{-AE}{6\,f(\alpha,\nu)} & \frac{-AE}{6\,f(\alpha,\nu)} & \frac{-AE}{6\,f(\alpha,\nu)} \\ 0 & 0 & -\frac{\sqrt{3}\,kAE}{6\,g(\alpha,\nu)} & \frac{\sqrt{3}\,kAE}{6\,g(\alpha,\nu)} & \frac{\sqrt{3}\,kAE}{6\,g(\alpha,\nu)} & -\frac{\sqrt{3}\,kAE}{6\,g(\alpha,\nu)} \\ \frac{kAE}{3\,g(\alpha,\nu)} & -\frac{kAE}{3\,g(\alpha,\nu)} & -\frac{kAE}{6\,g(\alpha,\nu)} & \frac{kAE}{6\,g(\alpha,\nu)} & -\frac{kAE}{6\,g(\alpha,\nu)} & \frac{kAE}{6\,g(\alpha,\nu)} \\ \frac{E\,\mathrm{I_p}}{6\,R\,g(\alpha,\nu)} & -\frac{E\,\mathrm{I_p}}{6\,R\,g(\alpha,\nu)} & \frac{E\,\mathrm{I_p}}{6\,R\,g(\alpha,\nu)} & -\frac{E\,\mathrm{I_p}}{6\,R\,g(\alpha,\nu)} & \frac{E\,\mathrm{I_p}}{6\,R\,g(\alpha,\nu)} & -\frac{E\,\mathrm{I_p}}{6\,R\,g(\alpha,\nu)} \\ 0 & 0 & -\frac{\sqrt{3}\,E\,w}{6\,f(\alpha,\nu)} & -\frac{\sqrt{3}\,E\,w}{6\,f(\alpha,\nu)} & \frac{\sqrt{3}\,E\,w}{6\,f(\alpha,\nu)} & \frac{\sqrt{3}\,E\,w}{6\,f(\alpha,\nu)} \\ \frac{E\,w}{3\,f(\alpha,\nu)} & \frac{E\,w}{3\,f(\alpha,\nu)} & \frac{-E\,w}{6\,f(\alpha,\nu)} & \frac{-E\,w}{6\,f(\alpha,\nu)} & \frac{-E\,w}{6\,f(\alpha,\nu)} & \frac{-E\,w}{6\,f(\alpha,\nu)} \end{bmatrix} \tag{41}$$

where $f(\alpha,\nu)$ and $g(\alpha,\nu)$ are given by:

$$\begin{aligned} f(\alpha,\nu) &= \cos^2\alpha - \nu\sin^2\alpha \\ g(\alpha,\nu) &= \sin 2\alpha\ (\nu+1) \end{aligned} \tag{42}$$

Note that the values of α for which the optimisation criterion tends to infinity in Fig. 7 are, precisely, the ones that make the columns of $\mathbf{W}$ equal zero; *i.e.* the values of α that solve for $f(\alpha,\nu)=0$ or $g(\alpha,\nu)=0$.

It is also interesting to note that, although it has not been required in the optimisation, for the configuration of Eq. (38) and for any α, the temperature is compensated for all the components of the wrench but the axial force. This statement can be checked adding all the elements of each row of matrix $\mathbf{W}^{-1}$ and noting that this sum is only different from zero for the first row. Thus,

$$\hat{\mathbf{t}} = \mathbf{W}^{-1}(\boldsymbol{\varepsilon}_m + \varepsilon_T\,\mathbf{1}) = \mathbf{W}^{-1}\boldsymbol{\varepsilon}_m + \varepsilon_T\,\frac{-AE}{f(\alpha,\nu)}(1,0,0,0,0,0)^T \tag{43}$$

Therefore, it is demonstrated that, for the current configuration, only the estimation of the first component of $\mathbf{t}$ (the axial force) is corrupted by a homogeneous temperature variation.

With the aim of analysing the observability of the wrench for different values of α, the covariance matrix of the wrench is estimated using Eq. (31). In order to represent the variance of each wrench component, the elements of the diagonal

covariance matrix divided by the measurement variance are shown in Eq. (44):

$$\begin{aligned} \frac{var(F_1)}{var(\varepsilon)} &= \frac{A^2\,E^2}{6\left(\cos^2\alpha-\nu\sin^2\alpha\right)^2} \\ \frac{var(F_2)}{var(\varepsilon)} = \frac{var(F_3)}{var(\varepsilon)} &= \frac{A^2E^2k^2}{3\sin^2 2\alpha\,(\nu+1)^2} \\ \frac{var(M_1)}{var(\varepsilon)} &= \frac{E^2\,\mathrm{I_p}^2}{6\,R^2\sin^2 2\alpha\,(\nu+1)^2} \\ \frac{var(M_2)}{var(\varepsilon)} = \frac{var(M_3)}{var(\varepsilon)} &= \frac{E^2\,w^2}{3\left(\cos^2\alpha-\nu\sin^2\alpha\right)^2} \end{aligned} \tag{44}$$

Fig. 8 represents the logarithm of the variance of the components of the wrench in terms of α for the configuration defined by Eq. (38) for $\nu = \frac{1}{3}$. Vertical lines for

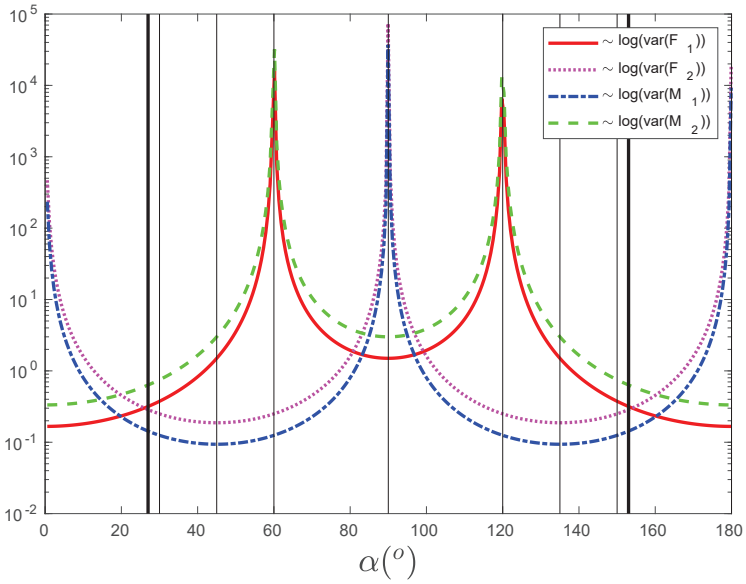

Fig. 8: The logarithm of the variance of the components of the wrench in terms of α for $\nu = \frac{1}{3}$ and unitary A, E, k, I_p, w and R.

α equal to 0°, 26.8°, 30°, 45°, 60° and 90° have been drawn in order to highlight the variance of each component for those angles. The figure clearly shows that the best orientation for the estimation of the axial force and bending moments happens for $\alpha = 0°$, while the best orientation for the estimation of the torsion moment and the shear forces happens for $\alpha = 45°$. The optimum value for measuring the whole wrench, $\alpha^{opt} = 26.8°$, is in between these angles. For the values of α equal to 0°, 60°, and 90°, the optimisation criterion tends to infinity, together with the variance of some wrench components.

5.2 Estimating $\mathbf{t}$ with 6 gauges constraining their location

The solutions obtained for the optimum α are not in general integer fractions of 180° and it can be difficult to bond the gauges to the shaft precisely for these orientations. Moreover, gauges are usually gathered in rosettes [6] where couples of gauges are shifted 90° or 60°. Using these rosettes can be a practical solution to make the bonding of the gauges easier and more precise, although the configurations will not be optimal any more.

With the objective of using rosettes, the optimisation problem of Eq. (35) can be solved with the following constraints:

- Three couples of strain gauges must be located at the same position (same φ value for each couple) as they will be part of the same rosette. Mathematically, the constraint can be written as:

$$\varphi_2 - \varphi_1 = \varphi_4 - \varphi_3 = \varphi_6 - \varphi_5 = 0 \tag{45}$$

- The orientations (δ_i and δ_j angles) of the gauges in each couple must be shifted a certain angle 2β (whose value will be set to 60° or 90°). Mathematically the constraint can be written as:

$$\delta_2 - \delta_1 = \delta_4 - \delta_3 = \delta_6 - \delta_5 = 2\beta \tag{46}$$

With the aim of providing insight into the symmetry of the optimal configurations, an angle γ is defined which establishes the orientation of the rosette by means of the middle-angle of the couple of gauges, as shown in Fig. 9. Then, the orientation of the gauges of the couple (i, j) can be written as $\delta_{(i,j)} = \gamma \pm \beta$.

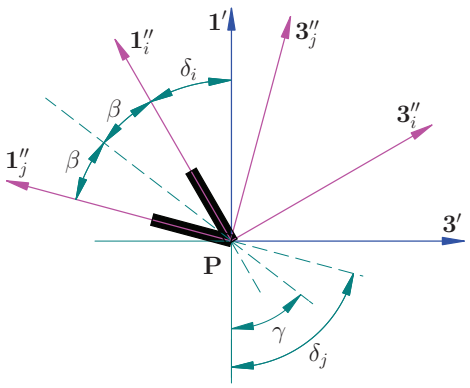

Fig. 9: Parameters γ and β for defining rosettes orientation.

An interesting result of these constrained optimisations (for $2\beta = 60^\circ$ and $2\beta = 90^\circ$) is that the solutions happen to be the configuration described by Eq. (38) for $\alpha = \beta$, $\gamma = 0$ and $\varphi_a = \varphi_b$. These results show that it is preferable to choose the configuration for $\alpha = 30^\circ$ over the one for $\alpha = 45^\circ$ because the former solution is much closer to the optimum one ($\alpha^{opt} = 26.8^\circ$).

Therefore, the 6-gauge configuration to be implemented with rosettes that minimises the constrained optimisation criterion is:

$$\begin{aligned} \boldsymbol{\varphi}^{opt} &= (0^\circ, 0^\circ, 120^\circ, 120^\circ, 240^\circ, 240^\circ) \\ \boldsymbol{\delta}^{opt} &= (30^\circ, -30^\circ, 30^\circ, -30^\circ, 30^\circ, -30^\circ) \end{aligned} \tag{47}$$

The gauges, for the configurations with $2\beta = 60^\circ$ and $2\beta = 90^\circ$, would be bonded in the shaft as shown in Fig. 10.

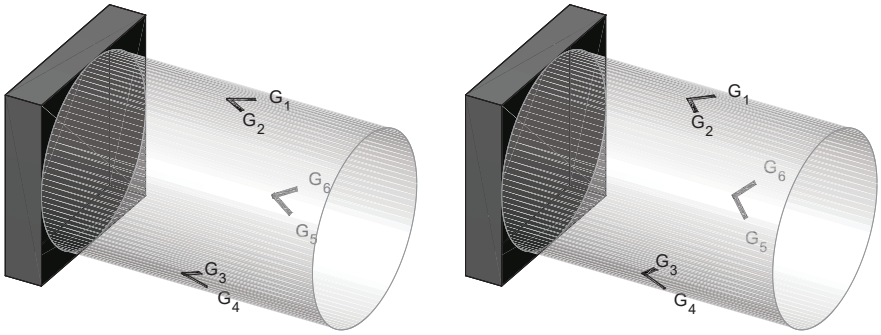

(a) 6-gauges configuration for $2\beta = 60^\circ$. (b) 6-gauges configuration for $2\beta = 90^\circ$.

Fig. 10: Optimal 6-gauges constrained configurations for the estimation of $\mathbf{t}$.

The difference between the optimum and these non-optimum configurations can be calculated by means of the variance of the estimation of the components of the wrench. Evaluating Eq. (44) for $\alpha = 30^\circ$, the variance of the components of $\mathbf{t}$ are:

$$\begin{aligned} \frac{var(F_1)}{var(\varepsilon)} &= \frac{8A^2E^2}{3(\nu-3)^2}, \quad \frac{var(F_2)}{var(\varepsilon)} = \frac{var(F_3)}{var(\varepsilon)} = \frac{4k^2A^2E^2}{9(\nu+1)^2} \\ \frac{var(M_1)}{var(\varepsilon)} &= \frac{2E^2Ip^2}{9R^2(\nu+1)^2}, \quad \frac{var(M_2)}{var(\varepsilon)} = \frac{var(M_3)}{var(\varepsilon)} = \frac{16E^2w^2}{3(\nu-3)^2} \end{aligned} \tag{48}$$

For $\alpha = 45^\circ$, the variance of the components of $\mathbf{t}$ are:

$$\begin{aligned} \frac{var(F_1)}{var(\varepsilon)} &= \frac{2A^2E^2}{3(\nu-1)^2}, \quad \frac{var(F_2)}{var(\varepsilon)} = \frac{var(F_3)}{var(\varepsilon)} = \frac{k^2A^2E^2}{3(\nu+1)^2} \\ \frac{var(M_1)}{var(\varepsilon)} &= \frac{E^2Ip^2}{6R^2(\nu+1)^2}, \quad \frac{var(M_2)}{var(\varepsilon)} = \frac{var(M_3)}{var(\varepsilon)} = \frac{4E^2w^2}{3(\nu-1)^2} \end{aligned} \tag{49}$$

Comparing the values of Eqs. (48) and (49), the variances for estimating axial and bending loads (F_1, M_2, M_3) are lower for $\alpha = 30^\circ$, while the variances for torsion and shear forces (M_1, F_2, F_3) are lower for $\alpha = 45^\circ$. In any case, the value of the optimisation criterion defined in Eq. (34) is lower value for the former configuration.

Finally, let us recall that when solving the optimisation problem for the determination of these solutions, temperature compensation has not been required. In the next section more gauges will be used in order to find optimal configurations in order to estimate $\mathbf{t}$ compensating for the temperature variations.

5.3 Estimating the components of $\mathbf{t}$ with 8 strain gauges

In order to obtain a symmetric configuration that compensates for temperature variations, 2 strain gauges are added to the previous set. With 8 gauges, an optimal configuration has been found constraining couples of gauges, as in the previous section, to be bonded together with the same value of φ and having a difference of 2β between their δ angles. The constraints can be mathematically written as:

$$\varphi_2 - \varphi_1 = \varphi_4 - \varphi_3 = \varphi_6 - \varphi_5 = \varphi_8 - \varphi_7 = 0 \tag{50}$$

$$\delta_2 - \delta_1 = \delta_4 - \delta_3 = \delta_6 - \delta_5 = \delta_8 - \delta_7 = 2\beta \tag{51}$$

With said constraints, the procedure proposed in Section 4 to obtain configurations with temperature compensation has been used for $2\beta = 60^\circ$ and $2\beta = 90^\circ$.

Running the optimisation procedure for $2\beta = 60^\circ$, it is observed that the optimal configurations depend on ν but all the solutions share a common structure that can be written as follows:

$$\begin{aligned} \boldsymbol{\varphi}^{opt} &= (0^\circ, 0^\circ, 90^\circ, 90^\circ, 180^\circ, 180^\circ, 270^\circ, 270^\circ) \\ \boldsymbol{\delta}^{opt} &= (\gamma+\beta, \gamma-\beta, -\gamma+\beta, -\gamma-\beta, \gamma+\beta, \gamma-\beta, -\gamma+\beta, -\gamma-\beta) \end{aligned} \tag{52}$$

where $\gamma = \gamma(\nu)$. For a reference value of $\nu = \frac{1}{3}$, the following configuration is obtained:

$$\begin{aligned} \boldsymbol{\varphi}^{opt} &= (0^\circ, 0^\circ, 90^\circ, 90^\circ, 180^\circ, 180^\circ, 270^\circ, 270^\circ) \\ \boldsymbol{\delta}^{opt} &= (-9.9^\circ, 50.1^\circ, 9.9^\circ, -50.1^\circ, -9.9^\circ, 50.1^\circ, 9.9^\circ, -50.1^\circ) \end{aligned} \tag{53}$$

while for different values of ν, slightly different values of γ are obtained for the fixed values of $\boldsymbol{\varphi}^{opt}$. This configuration matches the structure of Eq. (52) for $2\beta = 60^\circ$ and $\gamma = 20.1^\circ$.

Running the optimisation procedure for $2\beta = 90^\circ$, the resulting optimum configuration is:

$$\begin{aligned} \boldsymbol{\varphi}^{opt} &= (0^\circ, 0^\circ, 90^\circ, 90^\circ, 180^\circ, 180^\circ, 270^\circ, 270^\circ) \\ \boldsymbol{\delta}^{opt} &= (60^\circ, -30^\circ, 30^\circ, -60^\circ, 60^\circ, -30^\circ, 30^\circ, -60^\circ) \end{aligned} \tag{54}$$

regardless of the numerical values of the geometric and material parameters. Moreover, this configuration matches the structure of Eq. (52) for $2\beta = 90^\circ$ and $\gamma = 15^\circ$.

The configurations defined in Eqs. (53) and (54) are represented in Fig. 11. They both are remarkable strain gauge configurations since they have the following desirable properties:

- Rosettes can be used, ensuring an accurate angle between pairs of gauges.
- The rosettes are located 90° apart (in azimuth direction) making it easy to bond the rosettes precisely.
- The configurations compensate temperature variations without the need for any extra gauge or device.
- The configurations are optimum (given the constraints) which maximises the measuring sensitivity.
- The configurations are symmetric, which provides symmetric expressions for the estimation of the two bending moments and the two shear forces.

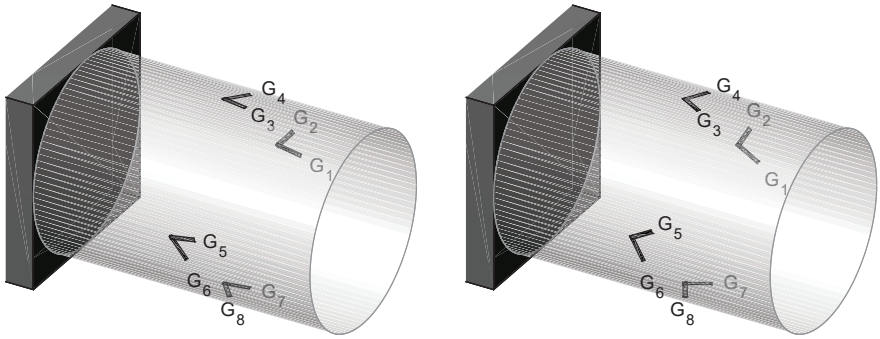

(a) 8-gauges configuration for $2\beta = 60°$. (b) 8-gauges configuration for $2\beta = 90°$.

Fig. 11: Optimal 8-gauges constrained configurations for the estimation of $\mathbf{t}$.

– The variances of the bending moments are equal to each other and the variances of the shear forces are also equal to each other.

Moreover, these configurations have an additional very interesting property regarding the robustness of a practical implementation. If a single strain gauge or a two-gauge rosette was damaged by accident, the 8 strain gauge configurations would still provide enough information to continue estimating all the components of the wrench as the rank of the $\mathbf{W}$ matrix would still be 6. However, the estimation with 6 strain gauges would fail to compensate thermal strains. In this situation, it would suffice to know which gauges have been damaged in order to perform the calculation of $\hat{\mathbf{t}}$ based on the rows of $\mathbf{W}$ related to the healthy strain gauges.

5.4 Table of Results

As a resume, results in Section 5 are shown in Table 1. The first column represents the number of strain gauges for each configuration; the second represents their position and orientation. Notice that writing the values of some optimum δ-s with a decimal point refers to the fact that those numbers are not integer values (when expressed in degrees) and the actual optimum value is approximated with one decimal. On the contrary the optimum values represented without the decimal point are precisely integer values. Continuing with the table, the third column indicates if the configuration automatically compensates *apparent strains* devoted to temperature variations; the fourth column indicates if constraints have been imposed to get the configuration; the last column indicates if the optimum configuration depends on the value of Poisson's modulus ν.

6 Preliminary experimental validation of the approach

In order to show that the presented theoretical approach can be used to measure the mechanical loads in circular section shafts, a test rig has been designed and built.

#	$\boldsymbol{\varphi}^{opt}, \boldsymbol{\delta}^{opt}$	T	C	$\delta^{opt}(\nu)$
6	$\boldsymbol{\varphi}^{opt} = (0°, 0°, 120°, 120°, 240°, 240°)$ $\boldsymbol{\delta}^{opt} = (26.8°, -26.8°, 26.8°, -26.8°, 26.8°, -26.8°)$	no	-	yes
6	$\boldsymbol{\varphi}^{opt} = (0°, 0°, 120°, 120°, 240°, 240°)$ $\boldsymbol{\delta}^{opt} = (30°, -30°, 30°, -30°, 30°, -30°)$	no	60°	no
6	$\boldsymbol{\varphi}^{opt} = (0°, 0°, 120°, 120°, 240°, 240°)$ $\boldsymbol{\delta}^{opt} = (45°, -45°, 45°, -45°, 45°, -45°)$	no	90°	no
8	$\boldsymbol{\varphi}^{opt} = (0°, 0°, 90°, 90°, 180°, 180°, 270°, 270°)$ $\boldsymbol{\delta}^{opt} = (-9.9°, 50.1°, 9.9°, -50.1°, -9.9°, 50.1°, 9.9°, -50.1°)$	yes	60°	yes
8	$\boldsymbol{\varphi}^{opt} = (0°, 0°, 90°, 90°, 180°, 180°, 270°, 270°)$ $\boldsymbol{\delta}^{opt} = (60°, -30°, 30°, -60°, 60°, -30°, 30°, -60°)$	yes	90°	no

Table 1: Optimum configurations for the wrench estimation.

6.1 Description of the test rig

The test rig consist of a shaft supported on bearings. One of the supporting bearings can be translated in order to introduce loads on the shaft. The shaft is rotated by an electric motor, which uses a variable-frequency drive to set the rotation velocity of the shaft at will. The strain and acceleration signals acquired on the rotating shaft are transmitted wireless to ground fixed bases. A PC is used to configure the acquisition system and collect all data. The actual test rig and a sketch of it are shown in Figures 12 and 13, respectively.

The strain gauges are located in the central part of the test rig, whose length is $L_2 + L_3 + L_4$. The lengths that define the shaft are $L_1 = 47mm$, $L_2 = 90mm$, $L_3 = 235mm$ and $L_4 = 92mm$. The hollow cylinder has an outer radius of $R = 40mm$ and an inner radius of $r = 38mm$. It is made of steel with $E = 210\,GPa$ and $\nu = 0.3$. The shaft is simply supported on a couple of bearings at points C_1 and C_2 located at one end. Moreover, the shaft is also supported on another bearing at point Q, which can be translated in the $\mathbf{y}$ direction (as depicted in Figure 13) by means of a leadscrew. This displacement is determined by coordinate y and introduces a shear force and a bending moment on the shaft. **A** and **B** are the sections perpendicular to the shaft where the strain gauges have been bonded. In section **A** the 8-gauge configuration defined in Eq. (54) has been bonded. In section **B** a full- and a half-bridge have been bonded to measure the bending moments. These customary Wheatstone bridges are set to compare their outputs with the estimations of the 8-gauge configuration.

Precisely measuring the azimut of the rotation of the shaft (coordinate θ) is indispensable to obtain the wrench estimation in base xyz (recall Figure 5 for the definition of θ and bases xyz and 123). In order to obtain an estimation of θ, a triaxial wireless capacitive accelerometer has been used, which is fixed to the shaft and oriented as base 123.

There exist several methods to estimate θ as a function of the measured accelerations. For instance, if the angular velocity of the shaft is constant and sufficiently

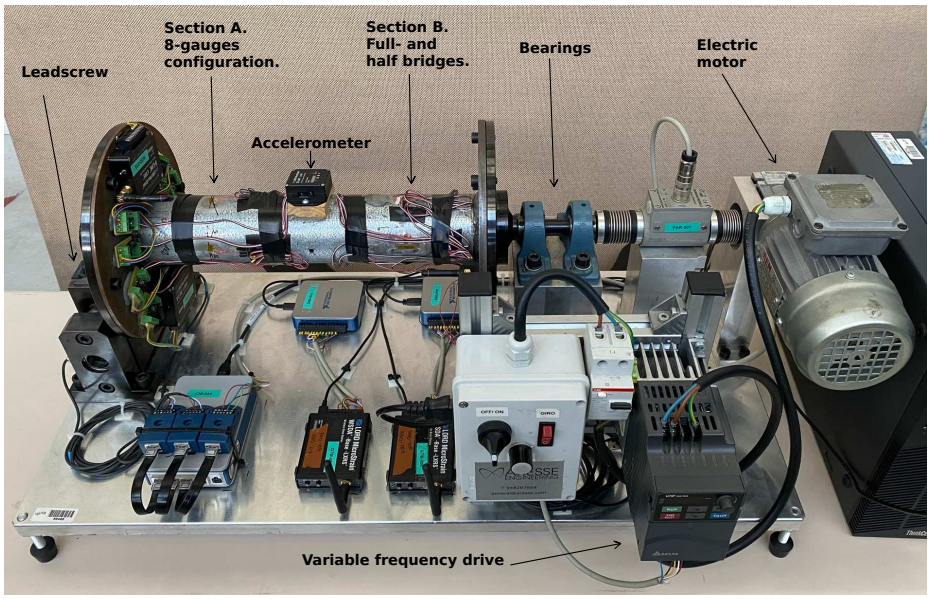

Fig. 12: The experimental test rig.

low, the accelerometers will only measure the gravity vector:

$$a_2 = g \sin\theta, \quad a_3 = g \cos\theta \tag{55}$$

where g is the modulus of gravity and a_2 and a_3 are the accelerations measured in directions 2 and 3, respectively. Calculating the four-quadrant inverse tangent of a_3 and a_2, an estimation of θ is obtained.

If the rotation of the shaft was faster or varied its velocity, the accelerometers would measure significant normal or tangent accelerations. In such cases more cumbersome procedures should be used to estimate angle θ.

The experiments performed with this test bed have been performed with a 100 Hz sampling frequency and in time intervals of 30 seconds.

6.2 Calibration of the customary Wheatstone bending bridges

In order to perform the calibration of the customary bending bridges at section **B**, the shaft has been released of the leadscrew becoming a rotating cantilever beam. This way a known point-load has been applied at **Q** (by means of gravity) which provides a bending moment with respect to section **A**. A set of four experiments have been performed with different known loads (besides the own weight of the shaft). Making the shaft rotate several rotations a sinusoidal signal is obtained at the output of the bending bridges with a certain amplitude and offset. These output signals of the full- and half bridges are provided by the acquisition system in mV/V.

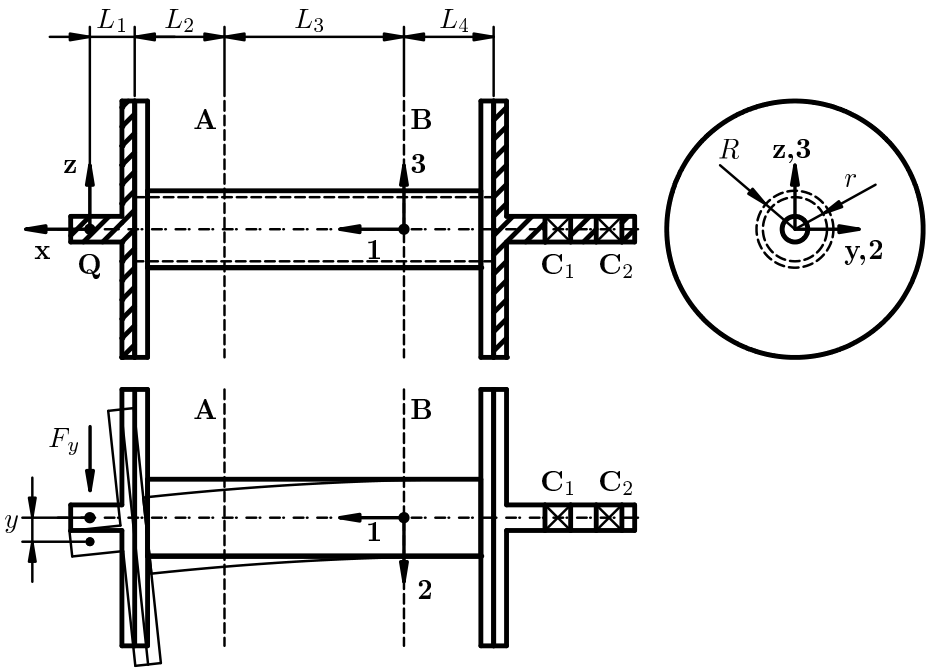

Fig. 13: Sketch of the shaft.

The calibration of the bending bridges has been performed subtracting these offsets to the signals and fitting a linear regression model between the amplitude values of these signals (in mV/V) and the applied loads (in Nm). Figure 14 shows the results of the linear regressions. The slope of the half bridge is approximately twice the slope of the full bridge, as the latter uses twice as many active strain gauges.

As a result of these experiments, calibrated relations are obtained between the bending moments at section **B** in base 123 and the outputs of the full- and half-bridges.

6.3 Calibration of the 8-gauges configuration

As the Wheatstone bridges, the 8 quarter bridges of the proposed configuration also need for a proper calibration. As in previous cases the amplitude and offset of the gauges signal has to be calibrated, but in this case the δ angles of the model that define the orientation of the strain gauges have to be calibrated too. Thus, the calibrated model will use calibrated values of δ slightly different from the nominal ones and the measured signals will be scaled and zeroed as in usual calibrations.

Assembling back the leadscrew for load application, an experiment has been done for a displacement of $y = 9\,mm$, leading to 8 signals (i.e. 8 vectors of 3000 strain measurements) measured in the quarter-bridges. The outputs of the full- and half-bridges are acquired too. In this experiment it will be assumed that force

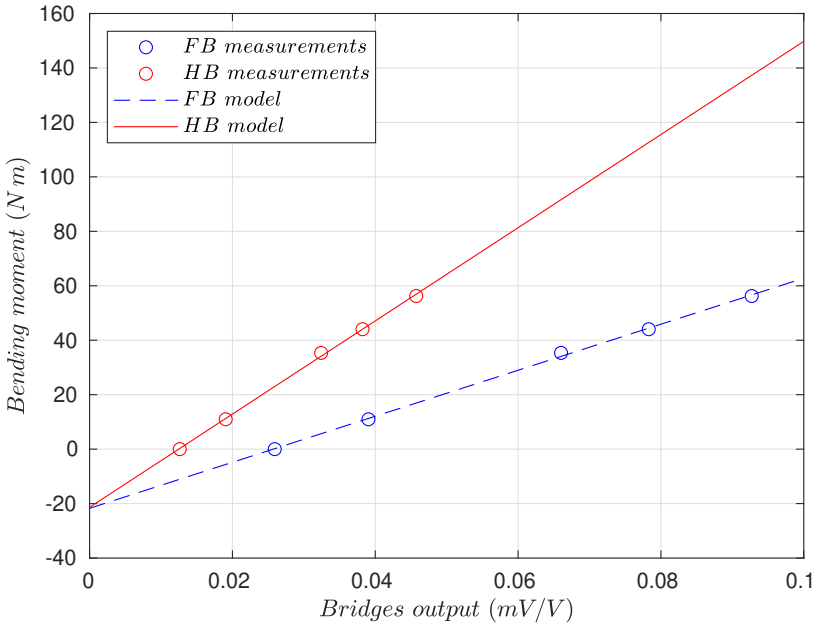

Fig. 14: Linear regressions of the full- and half-bridges.

F_1 and torsional moment M_1 are null. The calibrated measurements of the full- and half-bridges will be used to estimate the bending moments at section **B** in base 123. Assuming a point-load at **Q**, the applied forces (F_2 and F_3) and the bending moments at **A** (M_2^A and M_3^A) are calculated in terms of the measured bending moments at **B** (M_2^B and M_3^B) as:

$$\begin{aligned} F_2 &= \frac{M_3^B}{L_1+L_2+L_3}, \quad M_3^A = F_2\,(L_1+L_2) = M_3^B\,\frac{L_1+L_2}{L_1+L_2+L_3} \\ F_3 &= -\frac{M_2^B}{L_1+L_2+L_3}, \quad M_2^A = -F_3\,(L_1+L_2) = M_2^B\,\frac{L_1+L_2}{L_1+L_2+L_3} \end{aligned} \tag{56}$$

The intention of the design was that the leadscrew applied a point force at **Q** only in the horizontal y direction. However, due to missalignments and other possible inaccuracies of the test rig, the leadscrew also introduces a vertical component. This becomes evident when the moments are expressed in base xyz, which leads to a non zero M_y^A.

Based on the full- and half bridges at **B** it has been possible to determine the whole wrench at section **A** in bases 123 and xyz. As the wrench component in base xyz are nearly constant over θ, their mean values will be used to calibrate the quarter-bridges of the 8-gauges configuration. Multiplying the mean wrench (expressed in base 123) by $\mathbf{W}$ (as in Eq. (25)) we get the theoretical strains $\boldsymbol{\varepsilon}_t$ that one should measure at the 8-gauges configuration for any value of θ in a complete rotation of the shaft.

$$\boldsymbol{\varepsilon}_t(\theta) = \mathbf{W}\,\mathbf{t}(\theta) \tag{57}$$

These theoretical strains will be used in the calibration of the 8-gauges configuration that will follow the next 7 steps:

1. For $i = 1, \ldots, 8$, fit the i^{th} measured signal $\boldsymbol{\varepsilon}_m^i$ with the following linear regression model:
$$\boldsymbol{\varepsilon}_m^i = A_m^i \cos\boldsymbol{\theta} + B_m^i \sin\boldsymbol{\theta} + C_m^i \mathbf{1} \tag{58}$$
where A_m^i, B_m^i and C_m^i are the parameters for the i^{th} gauge, $\mathbf{1}$ is a vector of ones and vector $\boldsymbol{\theta}$ are the azimut values of the shaft for each time instant.
2. Estimate the amplitude X_m^i and phase shift η_m^i of each signal in terms of the estimated parameters A_m^i and B_m^i as:
$$X_m^i = \sqrt{(A_m^i)^2 + (B_m^i)^2}, \qquad \tan(\eta_m^i) = \frac{B_m^i}{A_m^i} \tag{59}$$
so that the strain signals can be rewritten as:
$$\boldsymbol{\varepsilon}_m^i = X_m^i \cos(\boldsymbol{\theta} - \eta_m^i) + C_m^i \mathbf{1} \tag{60}$$
3. Repeat steps 1 and 2 with the theoretical strains ($\boldsymbol{\varepsilon}_t$) to get the corresponding amplitudes X_t^i, phase shifts α_t^i and offsets C_t^i.
4. Calibrate the theoretical values of $\boldsymbol{\delta}$ of the model to minimise the difference between η_m^i and η_t^i. Let $\boldsymbol{\delta}^*$ be the calibrated $\boldsymbol{\delta}$ vector.
5. Using $\boldsymbol{\delta}^*$ recalculate the theoretical signals as:
$$\boldsymbol{\varepsilon}_{t,cal}(\theta) = \mathbf{W}(\boldsymbol{\delta}^*)\, \mathbf{t}(\theta) \tag{61}$$
Since $\boldsymbol{\varepsilon}_{t,cal}$ are calculated using a calibrated model, they will be named *theoretical calibrated strains*.
6. Recalculate the values of the parameters X_t^i and C_t^i as in step 3 (but using $\boldsymbol{\varepsilon}_{t,cal}$ instead of $\boldsymbol{\varepsilon}_t$) to get $X_{t,cal}^i$ and $C_{t,cal}^i$.
7. Calculate the calibrated measurement signals as:
$$\boldsymbol{\varepsilon}_{m,cal}^i = \frac{X_{t,cal}^i}{X_m^i}(\boldsymbol{\varepsilon}_m^i - C_m^i \mathbf{1}) + C_{t,cal}^i \mathbf{1} \tag{62}$$

Following this calibration procedure using the data of the experiments, the performance of the customary bridges and the 8-gauges configuration can be compared. Figure 15 compares the theoretical strains ($\boldsymbol{\varepsilon}_t$) calculated in Eq. (57) and the theoretical calibrated strains ($\boldsymbol{\varepsilon}_{t,cal}$) calculated by the calibrated model in Eq. (61). This figure shows that small errors bonding the gauges in the nominal orientation could lead to significant errors in strain amplitude. Moreover, Figure 16 compares the calibrated measurement signals ($\boldsymbol{\varepsilon}_{m,cal}$) calculated in Eq. (62) and the theoretical strains calculated by the calibrated model ($\boldsymbol{\varepsilon}_{t,cal}$) in Eq. (61). This figure shows how the calibrated model can represent the measured data.

Using the calibrated measured strains ($\boldsymbol{\varepsilon}_{m,cal}$) and the calibrated observation matrix ($\mathbf{W}(\boldsymbol{\delta}^*)$), it is possible to estimate the complete wrench at section $\mathbf{A}$ by means of the 8-gauge configuration as:
$$\hat{\mathbf{t}} = \left(\mathbf{W}(\boldsymbol{\delta}^*)^T \mathbf{W}(\boldsymbol{\delta}^*)\right)^{-1} \mathbf{W}(\boldsymbol{\delta}^*)^T \boldsymbol{\varepsilon}_{m,cal} \tag{63}$$

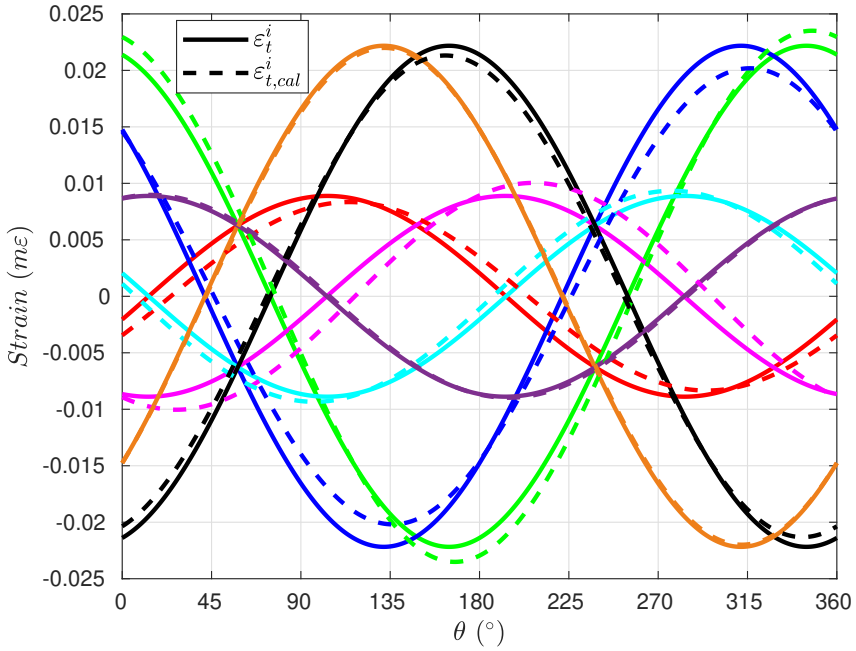

Fig. 15: Theoretical strains calculated with nominal $\boldsymbol{\delta}$ and $\boldsymbol{\delta}^*$.

Writing this wrench in the xyz base, it can be compared to the one estimated in terms of the customary full- and half-bridges. The force applied by the leadscrew and the bending moment with respect to section **A** are shown in Figure 17.

It can be observed that the mean values of the bending moments estimated in terms of the customary bridges ($mean(M_z^{cb}) = -62.5\,Nm$) and the 8-gauges configuration ($mean(M_z^{8g}) = -63.7\,Nm$) are very similar to each other, while the standard deviation of the 8-gauge configuration is higher ($std(M_z^{cb}) = 4.65\,Nm$ and $std(M_z^{8g}) = 6.64\,Nm$). The mean values of the force estimations are also similar ($mean(F_y^{cb}) = -454.36\,N$ and $mean(F_y^{8g}) = -443.96\,N$) and the 8-gauges configuration estimation also shows a higher dispersion ($std(F_y^{cb}) = 33.81\,N$ and $std(F_y^{8g}) = 51.86\,N$). The reason for this can be that section **A** is closer to point **Q** than section **B**, which leads to a smaller bending moment at **A**. Moreover, it is important to emphasise that while in the customary bridges case the force is calculated in terms of the bending moment measurements (no shear force bridge has been used) in the 8-gauges configuration the force is calculated directly.

7 Considerations for a practical implementation

In the previous sections a procedure has been developed in order to get optimal strain gauge configurations to measure the wrench components with the minimum possible variance, which has been the objective of this research. However, the

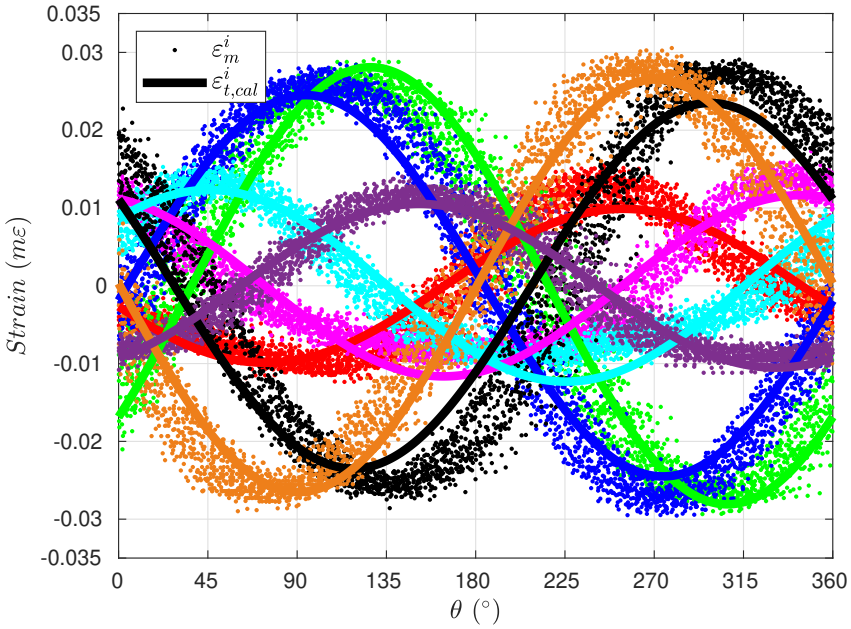

Fig. 16: Calibrated measured strains ($\boldsymbol{\varepsilon}_{m,cal}$) compared to the theoretical calibrated strains ($\boldsymbol{\varepsilon}_{t,cal}$).

obtained results are far from being practically implementable as-is and further research would be necessary in the way towards designing a fully functional wrench measuring device.

One reasonable concern for the practical implementation can be not to know which is the sensitivity of the approach to the uncertainty of the parameters and measurement noise. In fact, performing this analysis is mandatory to know *a priori* the range of uncertainty in the estimation of the wrench components.

For a complete validation of the approach, at least for some of the optimal configurations obtained in the results, a calibration procedure should also be designed in order to be able to correct the measurement errors to an acceptable level. As in this approach all the strain gauges contribute to measure all the wrench component, a dedicated calibration procedure should be designed taking into account the particular characteristics of the measuring device. Although a calibration procedure has been presented in the previous section, further research would be necessary to obtain a simpler and more robust calibration procedure for the 8-gauges configuration.

The practical implementation of an experimental set up has brought to light some practical inconveniences that might compromise the application of the approach, as the need for a cumbersome calibration procedure. Some other issues could appear in practical implementations where the axial force and moment played an important role. These issues are fundamental for the implementation

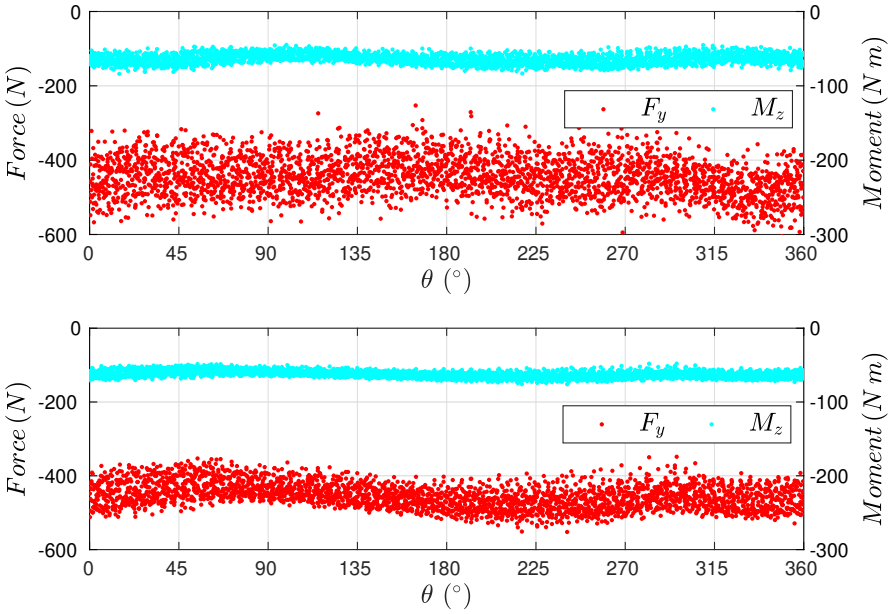

Fig. 17: Estimation of F_y and M_z based on the 8-gauge configuration (top) and the customary bridges (bottom).

of a full functionality measuring device but they have not been tackled in this paper and remain as future work.

8 Conclusions

In this paper a new approach for mechanical load measurement in circular cross-section shafts has been presented. The first step has been to write an expression for the strain of an arbitrarily located gauge in terms of the mechanical loads (forces and moments) exerted on the shaft. This expression is useful by itself, providing insight into the relation between the strain of a gauge, its location and the components of the mechanical loads exerted on the shaft.

While it is customary to measure mechanical loads with Wheatstone full- or half-bridges, it has been shown that measuring the strain of individual gauges with quarter-bridges provides the opportunity to use the measured strain of a single gauge in the estimation of several load components. Using the functional relation between the strain of a gauge and the load exerted on the shaft, a procedure has been developed in order to determine the optimal location of a set of strain gauges to estimate the six components of the wrench. The most innovative characteristic of the approach is that all the strain gauges contribute to the estimation of each component. Consequently, each load component is estimated as a different linear combination of the strains measured in the individual gauges.

Results show that it is possible to estimate the 6 load components using only 6 strain gauges while the state of the art used 24 gauges (4 for each load component). This is a remarkable reduction in the number of gauges that can substantially reduce the cost of applications that require to measure the 6 load components.

As the *apparent strain* is a common inconvenience in mechanical load estimation with strain gauges, the procedure for strain gauge placement has been extended in order to take this effect into account and provide robust configurations that are insensitive to temperature variations.

Additionally, as a precise orientation of the gauges can be difficult when bonding them, the procedure has been further extended to provide configurations where rosettes of gauges can be used. This approach provides accuracy in the relative angle between couples of strain gauges and divides by two the number of bonding operations on the shaft.

With each of the two optimal 8-gauge configurations obtained, it is possible to optimally estimate, with temperature compensation, the 6 load components exerted on a circular cross-section shaft, which to best of authors knowledge has not been reported in the literature.

A preliminary experimental validation of one of the 8-gauge configurations has been performed. The experiments have shown the effectiveness of the approach. However, the estimation results show a considerable dispersion which makes evident the complexity of the experimental implementation of the approach compared to the simplicity of its theoretical development.

Finally it is important to note that the approach proposed in this paper opens the possibility to obtain optimal solutions with a bigger number of strain gauges. Moreover, it is also possible to further extend the presented procedures in order to address other load measuring problems with different characteristics. For example, while the procedure has been developed only for circular cross-section shafts, the formulation could be further developed for other cross-section geometries.

Acknowledgements This work was funded by the "Convocatoria de ayudas a proyectos de I+D del Gobierno de Navarra" under the projects Ref. 0011-1365-2016-000092 and Ref. 0011-1365-2019-000094.

References

1. Aster, R., Borchers, B., Thurber, C.: Parameter Estimation and Inverse Problems (2013)
2. Bezziccheri, M., Castellini, P., Evangelisti, P., Santolini, C., Paone, N.: Measurement of mechanical loads in large wind turbines: Problems on calibration of strain gage bridges and analysis of uncertainty. Wind Energy **20**(12), 1997–2010 (2017). DOI 10.1002/we.2136. URL https://onlinelibrary.wiley.com/doi/abs/10.1002/we.2136
3. Cowper, G.R.: The shear coefficient in timoshenkos beam theory. Journal of Applied Mechanics **33**(2), 335–340 (1966)
4. Dally, J.W. and Riley, W.F. and McConnell, K.G.: Instrumentation for Engineering Measurements. Wiley (1993)
5. Draper, N.R., Smith, H.: Applied Regression Analysis. Wiley, New York (1998)
6. Hoffmann, K.: An Introduction to Stress Analysis and Transducer Design Using Strain Gauges. HBM (2012)
7. Hutchinson, J.R.: The shear coefficient in timoshenkos beam theory. Journal of Applied Mechanics **68**(1), 87–92 (2000)
8. Kay, S.M.: Fundamentals of statistical signal processing: estimation theory. Prentice-Hall, Inc., Upper Saddle River, NJ, USA (1993)

9. Kincaid, R.K., Padula, S.L.: D-optimal designs for sensor and actuator locations. Computers & Operations Research **29**(6), 701–713 (2002). DOI https://doi.org/10.1016/S0305-0548(01)00048-X. URL http://www.sciencedirect.com/science/article/pii/S030505480100048X. Location Analysis
10. Klein, V., Morelli, E.: Aircraft system identification: theory and practice. AIAA Education Series (2006)
11. Liu, X., Yue, R.X., Chatterjee, K.: Geometric characterization of d-optimal designs for random coefficient regression models. Statistics & Probability Letters **159**, 108,696 (2020). DOI https://doi.org/10.1016/j.spl.2019.108696. URL http://www.sciencedirect.com/science/article/pii/S0167715219303426
12. Ljung, L.: System Identification: Theory for the User (2nd Edition). Prentice Hall PTR (1998)
13. Loutas, T., Bourikas, A.: Strain sensors optimal placement for vibration-based structural health monitoring. The effect of damage on the initially optimal configuration. Journal of Sound and Vibration **410**, 217–230 (2017). DOI https://doi.org/10.1016/j.jsv.2017.08.022. URL http://www.sciencedirect.com/science/article/pii/S0022460X17306259
14. Ramsay D.C.: Principles of Engineering Instrumentation. Butterworth-Heinemann (1996)
15. Rizal, M., Ghani, J.A., Nuawi, M.Z., Haron, C.H.C.: Development and testing of an integrated rotating dynamometer on tool holder for milling process. Mechanical Systems and Signal Processing **52-53**, 559–576 (2015). DOI https://doi.org/10.1016/j.ymssp.2014.07.017. URL http://www.sciencedirect.com/science/article/pii/S0888327014003069
16. Stephan, C.: Sensor placement for modal identification. Mechanical Systems and Signal Processing **27**, 461–470 (2012). DOI https://doi.org/10.1016/j.ymssp.2011.07.022. URL http://www.sciencedirect.com/science/article/pii/S0888327011003116
17. Sun, Y., Hollerbach, J.M.: Observability index selection for robot calibration. In: Proceedings of the IEEE International Conference on Robotics and Automation, pp. 831–836 (2008)
18. Swevers, J., Ganseman, C., Tükel, D.B., De Schutter, J., Van Brussel, H.: Optimal robot excitation and identification. Transactions on Robotics and Automation **13**, 730–740 (1997)
19. Templeman, J.O., Sheil, B.B., Sun, T.: Multi-axis force sensors: A state-of-the-art review. Sensors and Actuators A: Physical **304**, 111,772 (2020). DOI https://doi.org/10.1016/j.sna.2019.111772. URL http://www.sciencedirect.com/science/article/pii/S0924424719308842
20. Turner, J., Hill, M.: Instrumentation for Engineers and Scientists. Oxford Science Publications (1999)
21. Udwadia, F.E.: Methodology for Optimum Sensor Locations for Parameter Identification in Dynamic Systems. Journal of Engineering Mechanics **120**(2), 368–390 (1994). DOI 10.1061/(ASCE)0733-9399(1994)120:2(368)
22. Zhang, S., Yang, J., Li, Y., Li, J.: Identification of bearing load by three section strain gauge method: Theoretical and experimental research. Measurement **46**(10), 3968–3975 (2013). DOI https://doi.org/10.1016/j.measurement.2013.07.017. URL http://www.sciencedirect.com/science/article/pii/S0263224113003163
23. Zhou, G., Yi, T., Chen, B.: Innovative design of a health monitoring system and its implementation in a complicated long-span arch bridge. Journal of Aerospace Engineering **30**, B4016,006 (2016). DOI 10.1061/(ASCE)AS.1943-5525.0000603
24. Zhou, G., Yi, T., Zhang, H., Li, H.N.: Energy-aware wireless sensor placement in structural health monitoring using hybrid discrete firefly algorithm. Structural Control and Health Monitoring **22** (2014). DOI 10.1002/stc.1707